Biocatalytic Elimination of Pharmaceutics Found in Water With Hierarchical Silica Monoliths in Continuous Flow

Wassim Sebai, Sher Ahmad, Marie-Pierre Belleville, Alexis Boccheciampe, Perrine Chaurand, Clement Levard, Nicolas Brun, Anne Galarneau, José Sanchez-Marcano

HAL Id: hal-03659113
https://hal.science/hal-03659113

Submitted on 4 May 2022

Biocatalytic Elimination of Pharmaceutics Found in Water With Hierarchical Silica Monoliths in Continuous Flow

Wassim Sebai[1,2], Sher Ahmad[1], Marie-Pierre, Belleville[1], Alexis Boccheciampe[3], Perrine Chaurand[3], Clément Levard[3], Nicolas Brun[2], Anne Galarneau[2]* and Jose Sanchez-Marcano[1]*

[1]Institut Européen des Membranes, Univ Montpellier, CNRS, ENSCM, Montpellier, France, [2]Institut Charles Gerhardt Montpellier, Univ Montpellier, CNRS, ENSCM, Montpellier, France, [3]Aix Marseille Univ, CNRS, IRD, INRAE, CEREGE, Aix-en-Provence, France

Pharmaceutical products (PPs) are considered as emerging micropollutans in wastewaters, river and seawaters, and sediments. The biodegradation of PPs, such as ciprofloxacin, amoxicillin, sulfamethoxazole, and tetracycline by enzymes in aqueous solution was investigated. Laccase from *Trametes versicolor* was immobilized on silica monoliths with hierarchical meso-/macropores. Different methods of enzyme immobilization were experienced. The most efficient process was the enzyme covalent bonding through glutaraldehyde coupling on amino-grafted silica monoliths. Silica monoliths with different macropore and mesopore diameters were studied. The best support was the monolith featuring the largest macropore diameter (20 μm) leading to the highest permeability and the lowest pressure drop and the largest mesopore diameter (20 nm) ensuring high enzyme accessibility. The optimized enzymatic reactor (150 mg) was used for the degradation of a PP mixture (20 ppm each in 30 ml) in a continuous recycling configuration at a flow rate of 1 ml/min. The PP elimination efficiency after 24 h was as high as 100% for amoxicillin, 60% for sulfamethoxazole, 55% for tetracycline, and 30% for ciprofloxacin.

Keywords: silica monolith, laccase, water treatment, enzyme immobilization, pharmaceutic micropollutant, X-ray micro-computed tomography

INTRODUCTION

Pharmaceutical products (PPs) are a group of hazardous contaminants found in wastewater in the concentration range of (ng L^{-1}–μg L^{-1}) (Halling-Sørensen et al., 1998; Björlenius et al., 2018; Burns et al., 2018). PPs can adversely impact both human health and aquatic life because of their recalcitrant nature even at low concentrations (Carlsson et al., 2006). A large variety of PPs are found in wastewater having different physicochemical properties; therefore, their removal from wastewater is a big challenge and versatile treatment techniques need to be developed (Jones et al., 2005; Bruce et al., 2010; de Jongh et al., 2012). Recently, advancement in wastewater treatment have resulted in the development of new treatment technologies for PP removal such as membrane separation, adsorption onto activated carbon, and advanced oxidation processes (AOPs) (Grandclément et al., 2017; Rajapaksha et al., 2019; Rocha et al., 2020).

Recently, oxidoreductase enzymes have been employed for the degradation of many recalcitrant PPs in wastewater. Indeed, oxidoreductase enzymes have shown catalyzing complex chemical reactions with high efficiency and selectivity at mild operational conditions. Different oxidoreductase enzymes such as peroxidases, tyrosinase, and laccases have been studied for PP degradation; however, laccases obtained from fungi (Shraddha et al., 2011) are most commonly applied for PP degradation (Singh Arora and Kumar Sharma, 2010; Demarche et al., 2012; de Cazes et al., 2014a). The widespread application of laccase stems from its low selectivity and ability to catalyze the oxidation reactions of a range of substrates such as ortho- and para-diphenols, methoxy-substituted phenols, aromatic amines, phenolic acids, and several other compounds *via* a single-electron oxidation mechanism (Pype et al., 2019).

Enzymes in free state exhibit high activity; however, it becomes difficult to separate them from the reaction media after the reaction; therefore, it becomes very challenging to apply free enzymes in continuous processes (Gasser et al., 2014). Moreover, free enzymes have shown poor stability in large-scale implementation, making it difficult to justify their higher cost to use (Iyer and Ananthanarayan, 2008). To overcome such limitations, enzyme immobilization is mostly implemented in view to improve the stability and the reusability of the biocatalysts (Sheldon, 2007; Iyer and Ananthanarayan, 2008; Cabana et al., 2009; Sheldon and van Pelt, 2013; de Cazes et al., 2014b; Patel et al., 2014; Zhang et al., 2015; Zheng et al., 2016; Ji et al., 2017).

Enzyme immobilization on solid supports can be carried out through physical or chemical methods (Hartmann and Kostrov, 2013; Sheldon and van Pelt, 2013). Physical immobilization includes adsorption, entrapment, or encapsulation, while chemical immobilization includes covalent binding or cross-linking (Brady and Jordaan, 2009; Fernandez-Fernandez et al., 2013; Rodrigues et al., 2021). Physical adsorption is a relatively simple method for enzyme immobilization, but enzymes are generally leached after few cycles of reaction (Jesionowski et al., 2014). Although chemical immobilization results in partial deformations of the enzyme molecular shape, the bond between the enzyme and the support allows to improve the process reusability. Therefore, chemical immobilization, specifically covalent binding, is of great interest for industrial purposes (Arca-Ramos et al., 2016; Mohammadi et al., 2018; Bebić et al., 2020; Sadeghzadeh et al., 2020; Zdarta et al., 2020; Rodrigues et al., 2021).

During enzyme immobilization, the support material plays an important role in the efficiency of the whole process (Rodrigues et al., 2021). A variety of supports such as biosourced carbonaceous materials (Naghdi et al., 2017), polysulfone (Edwards et al., 2002), α-alumina membranes (de Cazes et al., 2014b), polyamide (Silva et al., 2007), silica (Luckarift et al., 2004; Galarneau et al., 2006; Zhu et al., 2007), and carbon nanotubes (Tavares et al., 2015) have been studied for laccase immobilization. Among these, membranes have shown a great efficiency due to their compatibility with the existing water/wastewater treatment facilities. However, the major, yet unavoidable, challenge of using membranes for wastewater treatment is membrane fouling and low enzymes loading due to their very low surface area ($<4\,m^2\,g^{-1}$).

In order to improve enzyme loading, inorganic mesoporous support materials with high surface area have been recently studied for enzyme immobilization and in particular for water treatment processes (Kumar and Cabana, 2016; Sadeghzadeh et al., 2020; Zdarta et al., 2020; Guardado et al., 2021). Inorganic mesoporous materials are characterized by pore diameters ranging from 2 to 50 nm, and pore volumes and surface areas up to $2–3\,ml\,g^{-1}$ and $1,500\,m^2\,g^{-1}$, respectively. Furthermore, the multiplicity of the synthesis methods, such as sol-gel, microwave, hydro- and solvothermal, precipitation in polar and nonpolar media, as well as sonochemical approaches, allows to obtain tailor-made mesoporous materials with desired properties (Davis, 2002; Fajula et al., 2005; Nakanishi and Tanaka, 2007; Lu et al., 2020). Due to the above-mentioned features, mesoporous materials still attract growing attention for application in various fields of science and engineering, including biomedicine, energy storage, separation, adsorption, catalysis, and biocatalysis (Ji et al., 2016; Taghizadeh et al., 2020).

Among inorganic supports, mesoporous silica is one of the most widely used for enzyme immobilization due to their outstanding properties such as high thermal and chemical resistance, highly porous structure, high surface area, and high enzyme loading efficiency. Moreover, silica contains hydroxyl groups, which facilitate their functionalization with organosilanes, and further coupling with cross-linking agents for covalent enzyme immobilization. Silica can be used in many different forms such as sol-gel silica, fumed silica, colloidal silica nanoparticles, and silica gels and have been extensively studied for the immobilization of different types of enzymes, as oxidoreductases, transferases, hydrolases, and isomerases (Yiu and Wright, 2005; Zhou and Hartmann, 2012; Hartmann and Kostrov, 2013; van den Biggelaar et al., 2017, 2019; Debecker, 2018). Although mesoporous silica has shown promising results in terms of enzyme loading, stability of process, and degradation of PPs, the major remaining challenge is to scale up the process and the process efficiency (Luckarift et al., 2004; Zhu et al., 2007; Cabana et al., 2009).

Chemistry in flow is a promising option for the implementation of catalytic reactions enabling process intensification and simplified workups. Efforts have been made for the design of efficient microreactors. Macro-/mesoporous monoliths (silica and titania) were used as supports for catalytic functions (El Kadib et al., 2009; Linares et al., 2012) and presented a much higher efficiency (4–10 times) in comparison to packed-bed columns made of purely mesoporous materials (xerogel) (Linares et al., 2012) or of ground monoliths (El Kadib et al., 2009) due to a better control of contact time and an efficient mixing of fluids. The monoliths productivity was 30–400 times higher than that of batch reactors.

For this research work, such silica monoliths with hierarchical macro-/mesoporosity (Galarneau et al., 2016b) have been synthesized as supports for enzyme immobilization in order to intensify the process of PP elimination. Enzymes were already successfully immobilized

in such monoliths showing high efficiency in flow conditions for synthesis, racemic resolution, or protein digestion (Szymańska et al., 2013, 2016a, 2016b; Zielińska et al., 2017; Hou et al., 2019; Strub et al., 2019; van der Helm et al., 2019; Baccour et al., 2020; Kowalczykiewicz et al., 2022). Nevertheless, to our knowledge, our research group is the first to study the immobilization of laccases in monoliths with the objective of a large-scale application like micropollutant degradation in wastewaters. Monoliths with macroporosity are interesting supports for large-scale applications because they can be crossed by a wide range of convective flow with a minimum pressure drop. Moreover, they present several advantages compared to classical solid supports (powders, pellets etc.). On the one hand, the fluid passes through the support, allowing an instantaneous separation between the biocatalyst and the fluid, and on the other hand a precise control of the flow can be realized to avoid the formation of boundary layers while controlling very precisely the contact time. In this study, different enzyme immobilization methods for laccase were compared. The biocatalytic activity of laccases immobilized in silica monoliths was evaluated as a function of meso- and macropore diameter. The best laccase-monolith bioreactor was used for the elimination of a mixture of pharmaceutical micropolluants found in waters in recycling continuous flow.

EXPERIMENTAL SECTION

Materials

Polyethylene glycol (PEG) (99%, 20 and 100 kDa), tetraethyl orthosilicate (TEOS) (99%), 3-aminopropyl-triethoxysilane (APTES) (99%), powder of laccase from *Trametes versicolor* (activity ≥ 0.5 U mg^{-1}), tetracycline (TC) ($\geq 98\%$), ciprofloxacin, amoxicillin, sulfamethoxazole, glutaraldehyde (25% v/v), and 2,2′-azino-bis(3-ethylbenzothiazoline-6-sulfonic acid) (ABTS) ($\geq 98\%$) were purchased from Sigma-Aldrich. Glyoxal (39% v/v) and poly(ethylene glycol) diglycidyl ether (PEGDGE) were purchased from TCI-Chemicals. The transparent heat shrinkable gain in fluoroethylenepropylene (FEP AWG ¼ 1.6) with diameters of 6.4 and 3.8 mm before and after shrinkage, respectively, was purchased from Castello, France.

Silica Monoliths Synthesis

Tetraethyl orthosilicate (20 g) was left at −19°C for 1 h. Water (24.560 g) was put in a 100 mL Erlenmeyer flask and (2.313 g) nitric acid (68%) was added. The mixture was stirred for 5 min at room temperature. Polyethylene oxide (PEO) of 20 or 100 kDa was added and stirred at room temperature until homogenization. The mixture was left at −19°C for 15 min to cool down the solution without freezing. The Erlenmeyer flask was then placed in an ice bath and the solution was stirred. TEOS coming from the freezer was directly added to the slurry and stirred for 30 min at 500 rpm to get a homogeneous mixture and a translucent solution. Final composition of the mixture in molar ratio was as follows: 1 Si/0.60 < EO Unit <0.65/0.26 HNO$_3$/

14.21 H$_2$O. Polyvinyl chloride (PVC) tubes of 8 mm diameter and 10 cm length were closed on one side with a cap, sealed with parafilm, and kept at −19°C in the freezer. The tubes are taken from the freezer and filled with the mixture of the ice bath. The tubes were then closed by caps and sealed with parafilm and left in a 4 L water bath at 40°C for 3 days. During this time, the phase separation and the sol-gel process took place to form the macroporous network of the monoliths. Then, the monoliths were removed from the molds and placed in a 1 L water bath at room temperature and washed with water until reaching a neutral pH.
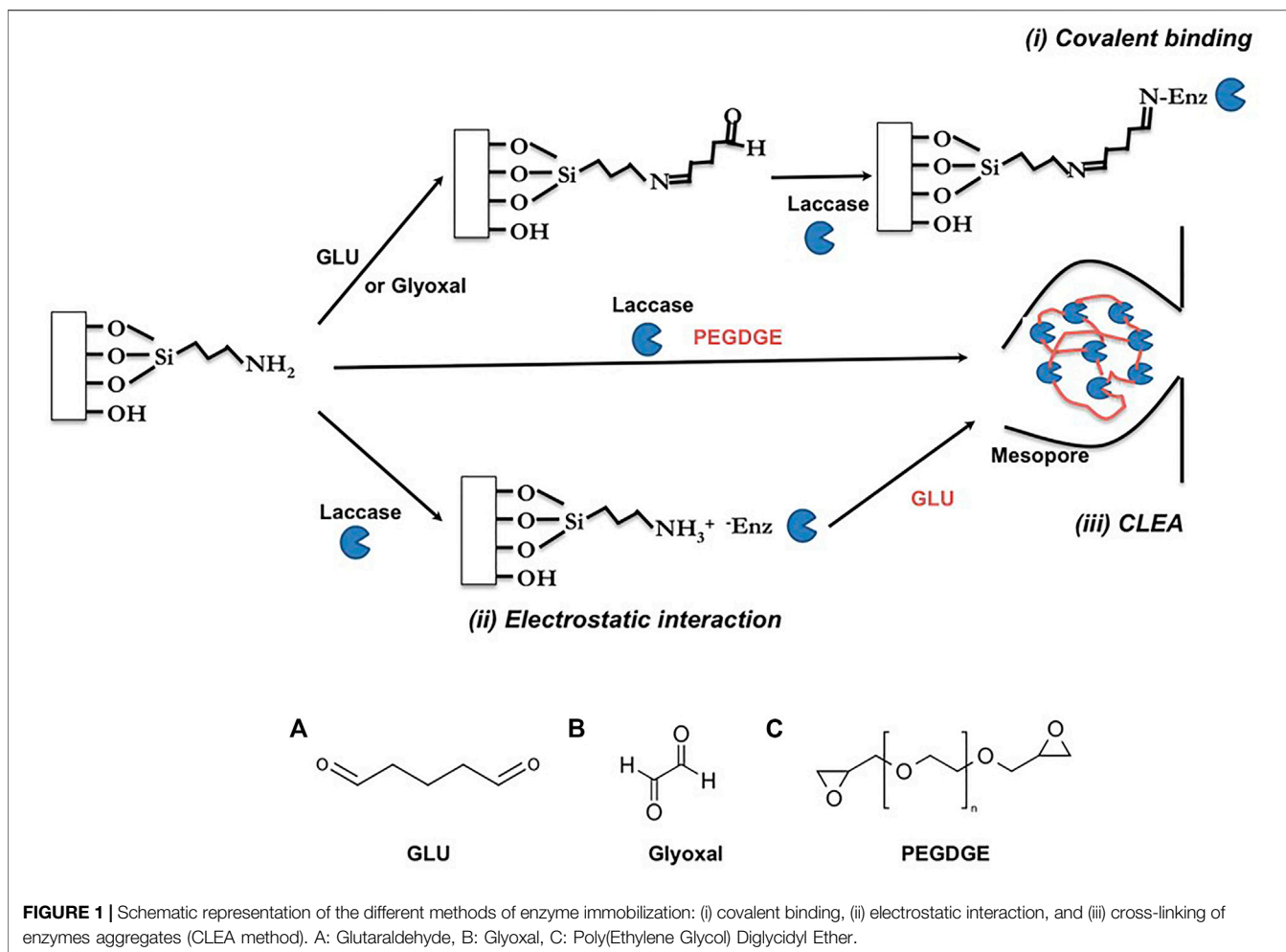
In order to obtain silica monoliths without mesopores, the monoliths were put in unsealed tubes and dried under specific conditions: 60°C for 24 h, then 80°C for 72 h followed by 120°C for 24 h (de Sousa Lima and Mohallem, 2021). The resulting monoliths were then calcined at 550°C for 8 h with a heating rate of 2°C min^{-1} from 25 to 550°C under air to remove remaining PEO.

To synthesize silica monoliths with mesopores, after the washing step until a neutral pH, monoliths were immersed in 1 L of aqueous ammonia (NH$_4$OH 0.1 M) in an autoclave and left in an oven at 40°C or 100°C for 24 h. The resulting monoliths were placed in a water bath and washed until a neutral pH (3 times 1 L of water) and then put in EtOH bath (500 ml) overnight for solvent exchange. The monoliths were then dried at room temperature overnight and calcined at 550°C for 8 h with a heating rate of 2°C min^{-1} from 25 to 550°C under air to remove the remaining PEO. Silica monoliths with a MCM-41 like mesoporosity have been synthesized by replacing the NH$_4$OH basic treatment by a NaOH treatment in the presence of cetyltrimethylammonium bromide (CTAB, Aldrich) with the molar composition of 1 Si/0.60 CTAB/0.20 NaOH/400 H$_2$O (Babin et al., 2007; Galarneau et al., 2016a). The autoclave was left at 115°C for 6 days. The same procedure of washing, drying, and calcination as above was applied. The hierarchical meso-/macroporous silica monoliths with different macropore (X μm) and mesopore (Y nm) diameters were named thereafter Si-X-Y. Silica monoliths of 0.6 cm diameter and 10 cm length were obtained and were cut at the desired lengths (0.5 cm) with a blade for further applications.

Aminopropyl-Grafted Silica Monoliths

Silica monoliths (0.7 g) were activated at 250°C under low vacuum nitrogen in order to eliminate adsorbed water and to ensure the repeatability of the grafting process. After 6 h of activation, the monoliths were immersed in 50 mL of absolute ethanol containing 1 mL of APTES and left overnight at 80°C under reflux. The resulting aminopropyl-grafted monoliths (NH$_2$-SiO$_2$) were then washed 3 times (30 min each) with 50 mL of absolute ethanol and dried at 80°C overnight. In order to optimize the amount of NH$_2$ functions at the surface of the silica monoliths, the volume of APTES was also varied to get a calibration curve.

NH$_2$-SiO$_2$ monolith of 0.6 cm diameter and 0.5 cm length was placed into two Inox tubes, which were put into the transparent heat shrinkable gain in FEP, before heated in the oven at 180°C for

FIGURE 1 | Schematic representation of the different methods of enzyme immobilization: (i) covalent binding, (ii) electrostatic interaction, and (iii) cross-linking of enzymes aggregates (CLEA method). A: Glutaraldehyde, B: Glyoxal, C: Poly(Ethylene Glycol) Diglycidyl Ether.

2 h to ensure the cladding of the monolith to produce the microreactor.

Immobilization of Laccase in the Aminopropyl Grafted-Silica Monoliths

Three different methods of enzyme immobilization were investigated with NH_2-SiO_2 monoliths: covalent bonding, electrostatic interaction, and adsorption followed by cross-linking [cross-linking of enzymes aggregates (CLEA) method] (**Figure 1**). Prior to the immobilization, an enzymatic solution was prepared with 5 g of enzymatic powder dispersed into 1 L of a citrate phosphate buffer solution (pH 7, 0.1 M). The solution was slowly agitated for 24 h at 25°C to ensure a complete rehydration of the enzymes. The activity of the enzymatic solution was measured by ABTS test (see below) and adjusted if necessary to 5 ± 1 U ml_{sol}^{-1}.

Covalent Bonding

For covalent bonding (**Figure 1**), two cross-linkers were used: glutaraldehyde (GLU) and glyoxal, which is less toxic than GLU. The protocol of immobilization was the same as previously reported (Ahmad et al., 2021). A solution (0.5 ml) of 4% (v/v)

GLU or glyoxal prepared in a citrate phosphate buffer solution (pH 7, 0.1 M) was put into contact with the cladded NH_2-SiO_2 monolith for 30 min. The monoliths were rinsed five times with 0.5 ml of the buffer solution to remove unreacted cross-linkers. Then, monoliths were filled with 0.4 ml of the laccase solution (5 ± 1 U ml_{sol}^{-1}). Enzymatic solution was introduced at the entrance of the tube-containing monolith allowing the penetration by capillarity. Then, the tube is closed and turned several times for 1 h. Afterwards, the monolith was rinsed with the buffer solution. The excess of the enzyme solution and the solutions resulting from the washings were collected to measure their activity and therefore to determine the amount of immobilized enzymes. After immobilization, enzymatic monoliths were stored in the buffer solution at 4°C.

Electrostatic Interactions

For the electrostatic interactions (**Figure 1**), two pH were studied, 5.5 and 7, for two durations 90 and 300 min. The cladded monolith was first impregnated with a buffer solution at pH 7 or pH 5.5. Then, 0.4 ml of enzyme solution at 5 ± 1 U ml_{sol}^{-1} prepared at pH 7 or 5.5 was passed through the tube containing monolith and left for 90 min or 300 min for both pH. Finally, the monolith was rinsed with the corresponding buffer solution.

CLEA Immobilization

For the CLEA method (**Figure 1**), GLU or poly(ethylene glycol) diglycidyl ether (PEGDGE) was used as cross-linker. Two different procedures were used for the different cross-linkers. For GLU, the enzymes were first adsorbed into the cladded monoliths at pH 7 for 90 min using the same protocol as for electrostatic interactions. Then, the monolith was rinsed with the buffer solution and 0.5 mL of GLU (4% v/v) was passed through the monolith and allowed to react for 30 min for GLU at room temperature. For the PEGDGE cross-linker, PEGDGE (1.4% v/v) was first introduced into the enzyme solution, which was then passed through the monolith and allowed to react for 24 h at 4°C, according to a previous protocol (Baccour et al., 2020). Finally, the monoliths were rinsed with the buffer solution.

Laccase Activity Assay

The activity ($A_{initial}$) of the free laccase was measured using 2,2′-Azinobis-(3-ethylbenzthiazoline-6-sulfonate) (ABTS) as substrate. One hundred microliters of the enzyme solution was added to 900 µL of a citrate phosphate buffer solution (pH 4, 0.1 M) containing 1 mM ABTS. The absorbance change of ABTS (transparent) into oxidized ABTS (blue) was measured every minute by UV-Vis spectrophotometry at 420 nm. The activity of the enzyme (in µmol min^{-1} mL^{-1} expressed as U mL^{-1}) was estimated by the Beer-Lambert law using the slope of the absorbance vs. time and the extinction coefficient of ABTS, ε = 3600 M cm^{-1}. The width of the curve was 1 cm.

The activity of immobilized enzymes in the monoliths can be determined by two ways, firstly by measuring the ABTS activity of the immobilized laccase in active monoliths ($A_{observed}$) (U mg$_{monolith}^{-1}$). This activity was measured by adding 5 mg of crushed monoliths to 25 mL of the ABTS solution (1 mM) in a 100 mL flask at 25°C under air and agitation. As previously mentioned, the activity was estimated by the change in the absorbance of ABTS solution vs. time.

Secondly, activity can be determined by calculating the amount of immobilized enzyme in the monoliths by the difference of activity in between the initial solution used for immobilization ($A_{initial}$) and the activity on the remaining laccase in solution (A_{left}) after immobilization plus the activity of the solutions used for the washings ($A_{rinsing}$). The enzyme immobilization yield ($\rho_{immobilization}$) was calculated using the following equations:

$$A_{immobilized} = A_{initial} - \left(A_{left} + \sum A_{rinsing}\right) \quad (1)$$

$$\rho_{immobilization} = \frac{A_{immobilized}}{A_{initial}} \times 100 \quad (2)$$

The efficiency of the immobilization was estimated according to **Eq. 3**:

$$\text{Efficiency} (\%) = \frac{A_{observed}}{A_{immobilized}} \times 100 \quad (3)$$

Pharmaceutical Micropollutant Removal

Pharmaceutical micropollutant degradation was carried out with 3 laccase-monolith reactors connected in series [0.6 cm diameter

and 0.5 cm length each with a biocatalytic (ABTS) activity of 5 U ± 0.5 U]. A mixture of four pharmaceutical molecules (ciprofloxacin, amoxicillin, sulfamethoxazole, and tetracycline) at 20 ppm each was prepared in osmosed water at pH 6 and put in a reservoir. Oxygen was bubbled in the reservoir containing 30 mL of this mixture in order to saturate the solution with oxygen. The solution was passed through the monoliths using a recirculation flow mode. The flow was ensured by an HPLC pump (Gibson model: 321, France) and was set at 1 mL min^{-1}. The temperature of the reservoir was set at 25°C. Aliquots of the solution were taken within time from the reservoir and analyzed by high-performance liquid chromatography coupled to triple quadrupole mass spectrometry (HPLC–MS). The aliquots were injected through a Macherey-Nagel C18 column (50 mm × 2 mm) with a Waters e2695 Separations Module, and the 410 m/z fragment was detected with a Micromass Quattro micro API device.

Permeability of Silica Monoliths

The permeability of NH$_2$-SiO$_2$ monoliths featuring different macropore diameters was carried out by passing osmosed water through the cladded monoliths at different flow rates. Silica monoliths of 0.6 cm diameter and 0.5 cm length were connected to a flow system consisting of an HPLC pump and a pressure gauge. The flow rate was increased from 0.5 to 15 mL min^{-1}. The backpressure exerted by the monoliths was measured using the pressure gauge. The flow rate (Q) in mL min^{-1} was expressed as Darcy rate (Q/A) in m h^{-1} considered as the fictive rate of the liquid through the total section (A) of flow, as if there was no porous network. The permeability (K) was calculated using Darcy's equation (**Eq. 4**) as follows:

$$K = \frac{Q}{A}\frac{l}{\Delta P}\mu \quad (4)$$

where K is the permeability coefficient (m^2), Q is the flow rate (m^3 s^{-1}), A is the cross section of the monolith (m^2), μ is the viscosity of the fluid ($\mu = 1.002$ mPas at 20°C for water), l is the length of the monolith, and ΔP is the difference of pressure at the outlet and inlet of the monolith (Pa).

Characterization Techniques

The physicochemical properties of the monoliths were characterized by nitrogen sorption at 77 K, TGA, ^{29}Si and ^{13}C MAS NMR spectroscopy, mercury intrusion, scanning electron microscopy (SEM), and x-ray micro-computed tomography (micro-CT).

The adsorption/desorption isotherms of nitrogen at 77 K were determined using a Micromeritics ASAP 2010 instrument. The samples (50 mg) were outgassed for 6 h in vacuum at 0.5 Pa and at 250 or 80°C for the native silica monoliths and the organo-functionalized monoliths, respectively. The mesopore diameters were calculated using the Broekhoff and De Boer (BdB) method, shown as one of the more accurate methods for silica materials (Galarneau et al., 1999). The specific surface areas of the monoliths were measured by the BET equation using the pressure range defined by the Rouquerol criteria (Rouquerol

et al., 2003). Mercury porosimetry experiments were carried out with a Micromeritics Autopore 9220 equipment by increasing the pressure from 0.0013 to 400 MPa. The mercury intrusion was performed with a monolith of 0.6 cm diameter and 1 cm length. Prior to the measurement, the sample was outgassed at room temperature for 10 min. The macropore diameters were determined by the Washburn-Laplace equation and the macro- and mesopore specific surface areas were calculated as shown previously (Didi et al., 2019). For silica materials, the mercury contact angle was set at 140° and the mercury surface tension was set at 0.485 N m⁻¹. Monolith morphology was studied using a Hitachi S-4800 I FEG-SEM Scanning Electron Microscope at "Plateau Technique de l'IEM laboratoire du Pole Chimie Balard Montpellier". 3D imaging of the macroporous network of the monoliths was performed by x-ray microcomputed tomography (micro-CT) with a microXCT-400 x-ray microscope (Zeiss). High-resolution scans were acquired at 40 kV and 250 μA. A total of 3,001 projections were collected through 360° sample rotation with an exposure time of 20 s per projection. A ×40 magnification optical objective was selected to achieve an isotropic voxel of 0.5 μm and a field-of-view (FOV) of $0.5 \times 0.5 \times 0.5 \ \mu m^3$. Volume reconstruction was performed with XMReconstructed-Parallel Beam-9.0.6445 software using a filtered back projection algorithm.

Avizo 8.0 software (Hillsboro, OR, United States) was used for the visualization, processing, and analysis of the reconstructed dataset. A simple thresholding step was first applied to isolate the pore network from the monolith solid and provide two binary volumes, showing the 3D organization of the (macro) pore network and solid phase respectively. The threshold value was determined at the intersection of the two main contributions of the histogram.

The (macro)porosity was expressed as $V_{pore \ network}/V_{total \ (pore \ network+solid)}$. Tortuosity was calculated using the Avizo module "centroid path tortuosity" on the "pore network" binary volume. First, centroids of the pore network were calculated for each orthoslice of the dataset along the x-, y-, or z-axis. Then, tortuosity was calculated by dividing the path length through the centroids by the straight length between the two ends of the path. The solid phase skeleton thickness and the macro pore size distribution were measured using the module "Auto Skeleton" (Avizo XSkeleton Extension) applied on the two binary volumes "solid phase" and "pore network" respectively. The Auto Skeleton module extracts from binary volume the centerline of interconnected regions (either the macro pore network or the solid fraction in this case). The obtained object is a 3D skeleton consisting of a set of segments connected through nodes. For each point of each segment, the distance to the nearest boundary is stored and averaged per segment. This average distance corresponds to either the average macropore radius or average half solid phase skeleton thickness.

The aminopropyl-grafted monoliths (NH₂-SiO₂) were examined by ²⁹Si MAS NMR, (¹H)-²⁹Si CP MAS NMR, and (¹H)-¹³C CP MAS NMR recorded with a 300-MHz Varian VNMRS300 (magnet "wide bore" of 7.05 T) and a probe Varian T3 MAS. Ten milligrams of ground monoliths was used to fill 7.5-mm ZrO₂ rotors and the samples were spinned

at 5 kHz. For ²⁹Si MAS NMR analysis, a π/6 pulse of 2 μs was used with a recycling time of 60 s. For (¹H)-²⁹Si CP MAS NMR analysis, a π/2 pulse of 6 μs and a contact time of 5 ms was used with a recycling time of 5 s. TGA was performed using Perkin Elmer STA 6000 in order to determine the amount of amino groups grafted on the monoliths by using the difference of weight loss between NH₂-SiO₂ monolith and native silica monolith, which takes into account the dehydroxylation of the monoliths. Ten milligrams of sample was heated from 40 to 900°C with a heating rate of 10°C/min under air flux. Elemental analysis was performed in order to validate the amount of grafted amino groups found by TGA. N, H, O, and C were analyzed using Elementar vario Micro Cube.

The bioactivity of the free enzymes and the enzymes immobilized on the silica monoliths was determined using spectroscopy UV-Vis at 420 nm using ABTS as substrate. The absorbance measurement was carried out using a spectrophotometer Shimadzu UV-2401 PC.

RESULTS AND DISCUSSION

Synthesis, Functionalization, and Characterization of Silica Monoliths
Control of Porosity

Silica monoliths of 0.6 cm diameter and 10 cm length exhibiting a homogeneous network of macropores as shown by SEM pictures (**Figure 2**) were synthesized by a combination of spinodal decomposition and sol-gel process using polyethylene oxide (PEO) of 20 and 100 kDa in acidic aqueous medium in the presence of tetraethyl orthosilicate (TEOS). The amount of EO/Si and the size of PEO were adapted to reach macropore diameters of 5, 10, and 20 μm (**Supplementary Figure S1**, **Table 1**).

The basic post-treatment (NH₄OH) of the monoliths transformed the silica oligomer network, issued from the acidic treatment, in an aggregation of silica nanoparticles into the skeleton (**Figure 2**). The size of the nanoparticles increased with the temperature and the duration of the basic treatment (Galarneau et al., 2016a). This induced a decrease in specific surface area (from 700 to 100 m²/g) and an increase in mesopore diameter (from 7 to 22 nm) for a temperature increase from 40 to 140°C (**Figure 3**). Monoliths with a mesopore diameter of 7, 10, and 20 nm were prepared with basic treatment at 40°C for 8 and 24 h, and at 100°C for 24 h, respectively (**Supplementary Figure S2**), leading to specific surface areas of approximately 700, 500, and 300 m²/g, respectively. Mercury porosimetry allowed to reveal the homogeneous distribution of macropore and mesopore diameters in the monoliths (**Figure 4**).

In order to obtain the effect of only the macropores in biocatalysis, monoliths with smaller mesopore diameter than the enzyme kinetic diameter (laccase kinetic diameter ~5–6 nm) were synthesized. A monolith with an MCM-41-like mesoporosity featuring ordered mesopores of 3 nm diameter was synthesized by replacing the NH₄OH basic treatment by a treatment in NaOH in the presence of surfactant CTAB at
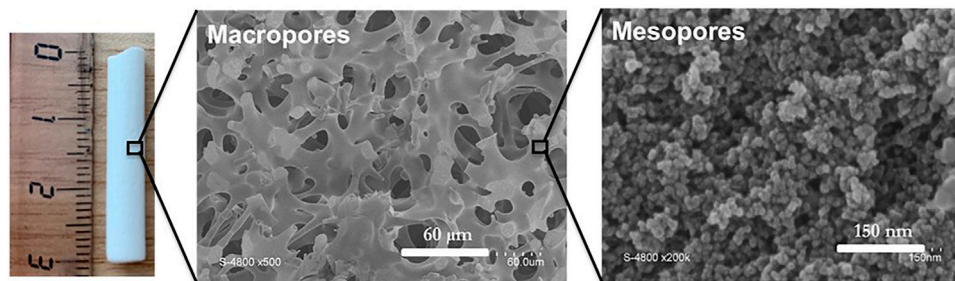
FIGURE 2 | Picture and SEM images of silica monolith Si-20-20.

TABLE 1 | Macropore diameter of silica monoliths Si-5-20, Si-10-20, and Si-20-20 determined by SEM, Hg-porosimetry, and micro-CT.

Monolith synthesis		Macropore diameter		
PEO (kDa)	EO/Si	D_{SEM} (µm)	$D_{Hg-poro}$ (µm)	$D_{micro-CT}$ (µm)
20	0.60	4	4.01 ± 0.05[a]	3.2
100	0.65	10	10.6 ± 0.7[a]	9.3
100	0.63	20	21.2 ± 3[a]	12.4

[a]Standard deviation taken at 50% of mean macropore diameter distribution.

115°C for 6 days (J. Babin et al., 2007). The specific surface area reached 830 m²/g as expected for an MCM-41 material (**Table 2**). However, during this synthesis, a second larger mesoporosity of approximately 15 nm diameter was noticed (**Supplementary Figure S3**). In order to obtain monoliths without mesopores, some monoliths were dried directly after the acidic step following a particular drying process (de Sousa Lima and Mohallem, 2021). The monolith featured a slightly lower diameter (0.5 mm instead of 0.6 mm) due to a larger shrinkage during the drying and the skeleton featured pores in the range of micropores to small mesopores (<5 nm) (**Supplementary Figure S3**). The macropore specific surface areas were calculated from Hg

porosimetry and were very low (<3 m²/g) (**Supplementary Figure S4**, **Table 2**).

The densities of the monoliths were given directly by Hg porosimetry software, but were also calculated using the porous volumes and the density of amorphous silica (ρ = 2.2 g cm⁻³). The monoliths with hierarchical meso-/macropores featured all densities of approximately 0.2 g cm⁻³, whereas the monolith obtained without basic treatment exhibited a higher density of approximately 0.4 g cm⁻³. Similarly, the porosities of the monoliths were calculated, and they exhibited a total porosity close to 0.9 (except for the monolith without basic treatment featuring a total porosity of 0.8) with a macroporosity of approximately 0.6–0.7.

The monoliths were further analyzed by x-ray micro-computed tomography (micro-CT) to assess the thickness of the skeleton, the length of a cell, and the macroporosity and the tortuosity of the macropores (**Figure 5**; **Table 3**). The 3D imaging was performed for monoliths of 0.6 cm diameter and 0.5 cm length. Pictures showed a homogeneous network of macropores (**Figure 5**). The tortuosity was approximately 1.3 and equal in all directions, supporting the homogeneity of the macropore network in the three space directions (**Table 3**). The monoliths were then decomposed into segments for both the
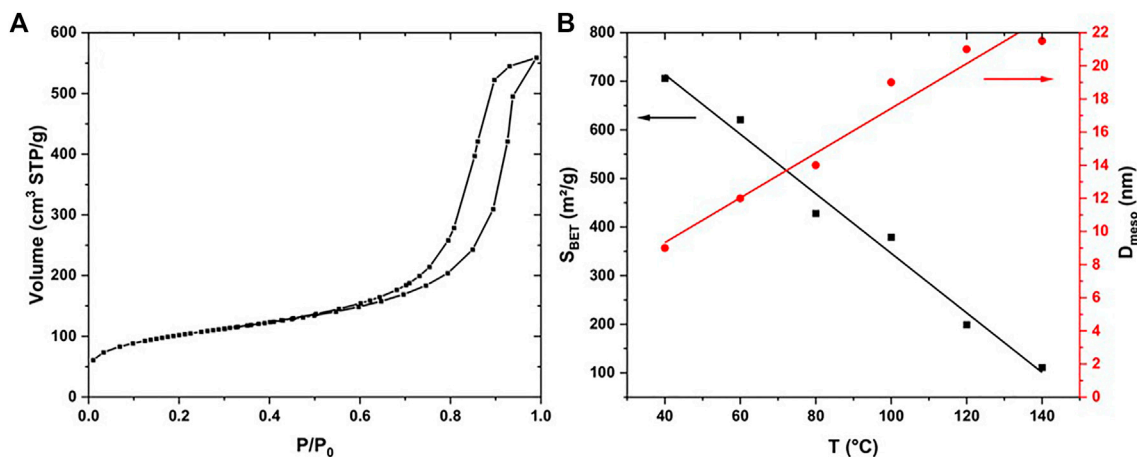

FIGURE 3 | (A) Nitrogen sorption isotherm at 77 K of silica monolith Si-20-20. **(B)** Evolution of mesopore diameter and specific surface area of silica monoliths as a function of temperature of NH₄OH post-treatment for 24 h.

FIGURE 4 | **(A)** Mercury porosimetry of silica monolith Si-20-20, **(B)** macropore size distribution, and **(C)** mesopore size distribution (pore diameter determined by the Washburn-Laplace equation).
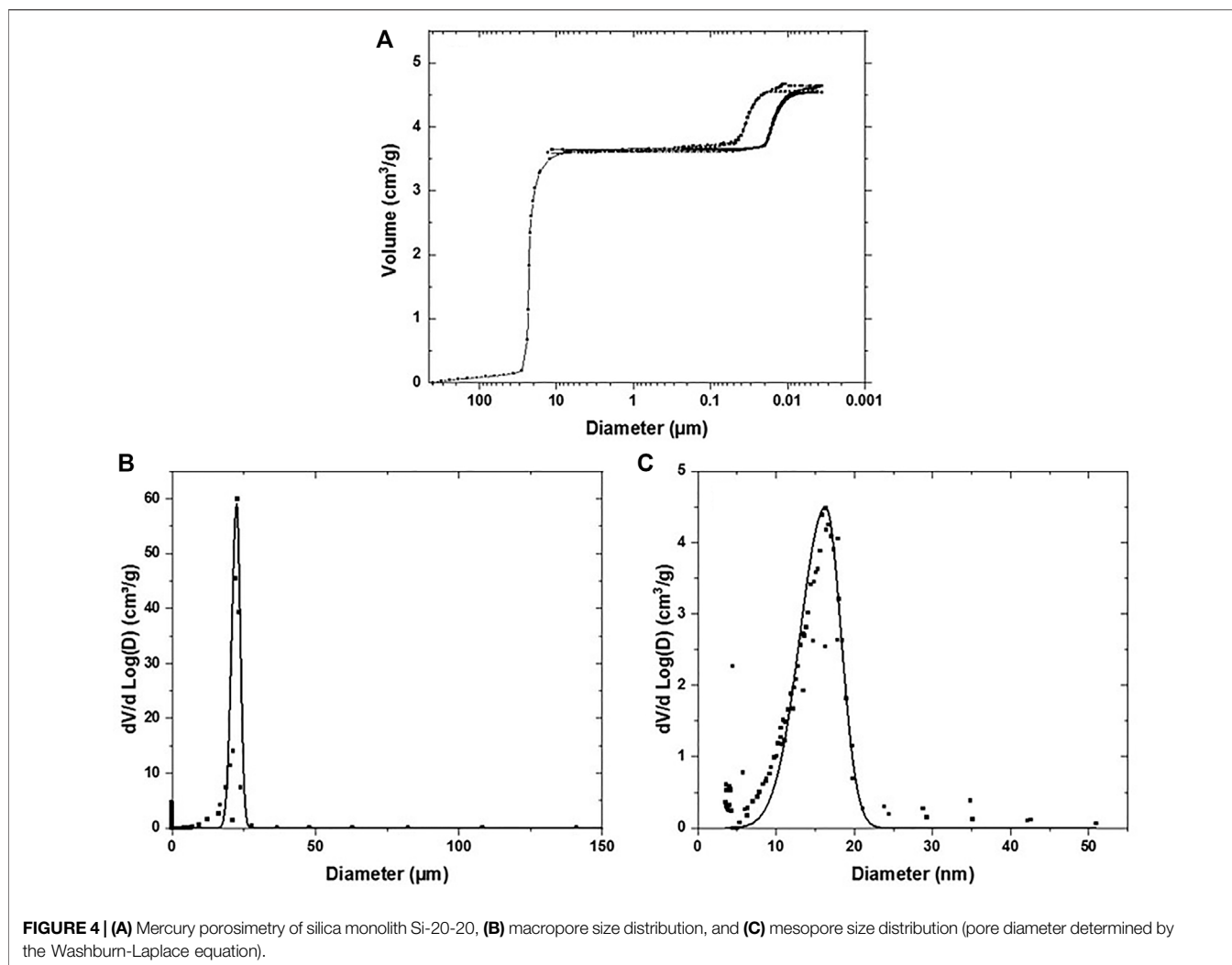
TABLE 2 | Textural characteristics of hierarchical meso-/macroporous silica monoliths Si-X-Y determined by nitrogen sorption at 77 K and by mercury porosimetry.

Si-X-Y	$D_{meso-Hg/N2}$[a] (nm)	$V_{meso-Hg/N2}$[a] (ml/g)	S_{BET-N2} (m^2/g)	$V_{macro-Hg}$ (ml/g)	$S_{macro-Hg}$ (m^2/g)
Si-20-20	16	0.87	369	3.41	0.67
Si-20-8	9	1.12	715	2.30	0.61
Si-5-20	15	0.94	361	2.25	2.43
Si-5-8	9	0.90	620	1.50	1.80
Si-20-(5<)[b]	4	0.35[b]	630	1.55	0.35
Si-20-(3,15)[c]	13	0.33 (15 nm)	830	3.00	0.56
	4	0.19 (3 nm)			

[a]For large mesopores (D > 15 nm) by intrusion of Hg and for small mesopores (D < 15 nm) by N_2 desorption isotherm and BdB method.
[b]Micro/mesopore volume: monolith without NH_4OH post-treatment featuring pores in the range of micropores and small mesopores < 5 nm.
[c]Monolith with MCM-41 (3 nm)-like mesoporosity featuring a secondary mesoporosity at 15 nm mesopore diameter.

macropore network and for the solid phase network. The distances from the middle of the segment to the edge of the skeleton or to the edge of the macropores were measured (**Figure 5**). More than 52,000 segments were analyzed to get the distribution lengths of the macropore diameters and the thickness of the skeleton (**Figure 5**; **Table 3**). Micro-CT 3D

image (stack of 1,000 2D orthoslices) is more representative than SEM 2D pictures, which used a maximum of 10 measures for macropore diameter and skeleton thickness (**Supplementary Figure S2**).

Good correlations were obtained between SEM, micro-CT, and Hg porosimetry (**Table 1**), except for the average macropore

FIGURE 5 | **(A)** Example of a binary volume obtained by micro-CT and thresholding, showing the 3D distribution of the macropore network x-ray tomography analysis of silica monolith Si-20-20. (1 vx = 0.5 μm). **(B)** Pore network skeleton obtained by applying the "Auto Skeleton" Avizo module. **(C)** Pore size distribution: number of segments vs. mean radius of each segment between two nodes.
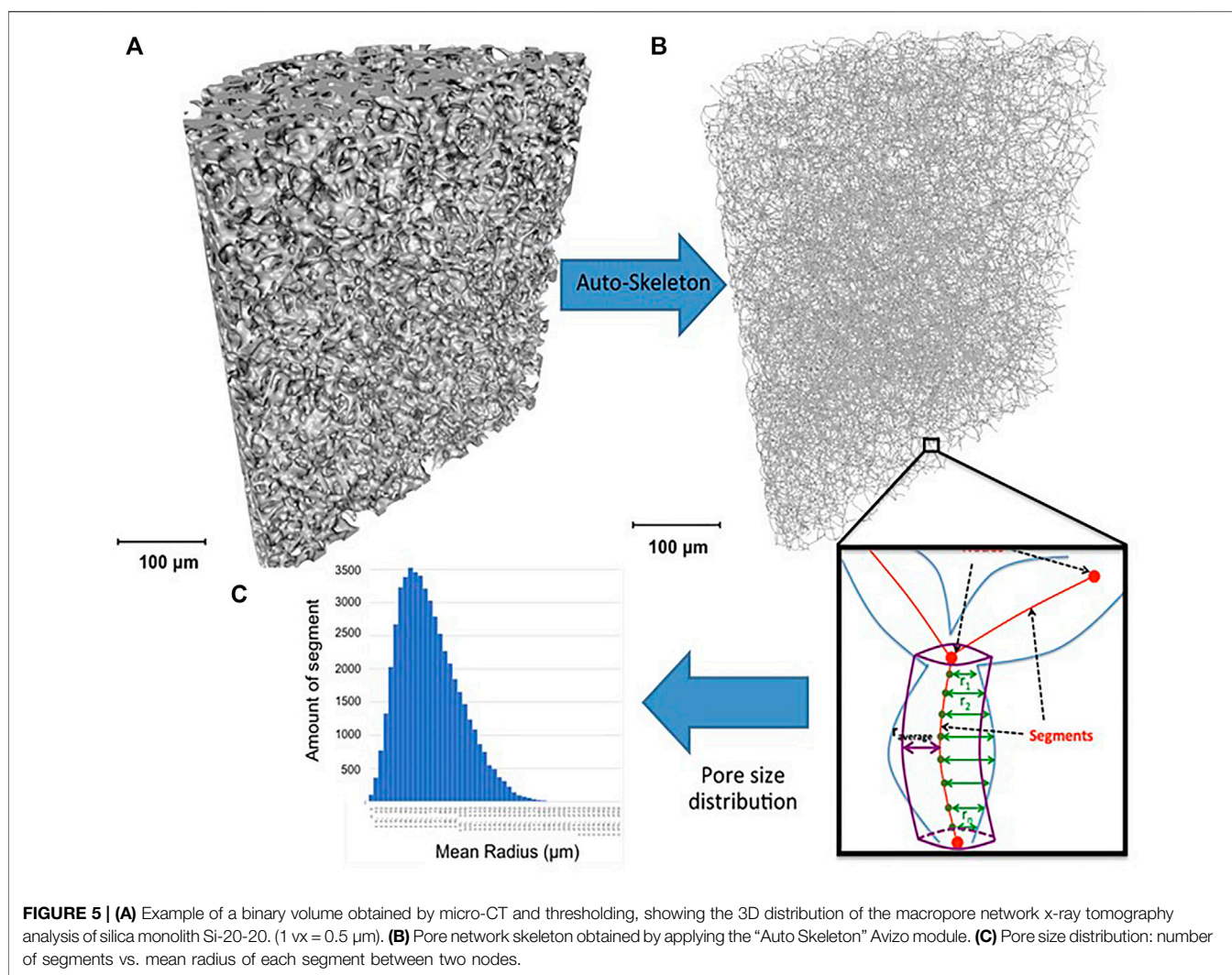
TABLE 3 | Textural characteristics of hierarchical meso-/macroporous silica monoliths Si-X-Y determined by micro-CT: macropore diameter, solid phase skeleton thickness, segment lengths of a cell between two nodes for the macroporosity and the solid phase skeleton, macroporosity, and tortuosity.

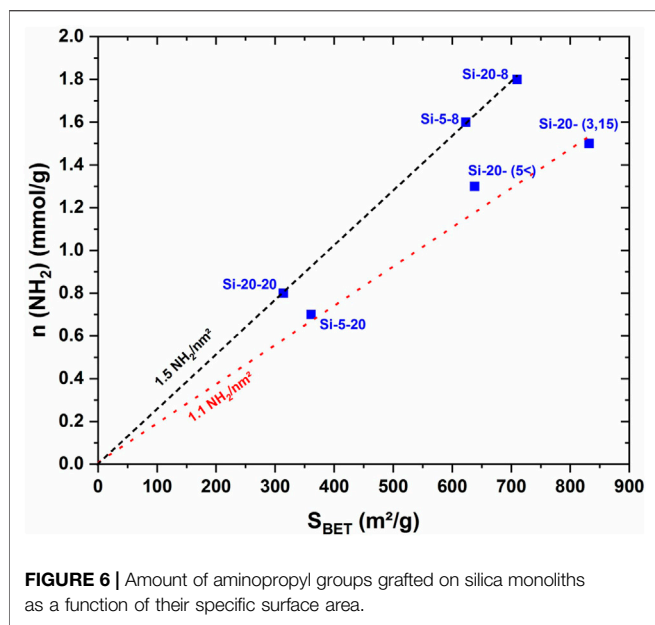| Si-X-Y	Si-20-20	Si-10-20	Si-5-20
D_{macro} (μm)	12.4	9.3	3.2
$L_{Segment-Macro}$ (μm)	12.3	9.8	5.3
$D_{skeleton}$ (μm)	7.1	5.8	2.3
$L_{Segment-Skeleton}$ (μm)	12.5	9.4	5.0
ε_{macro}	0.65	0.62	0.57
$\tau(x)$; $\tau(y)$; $\tau(z)$	1.26; 1.36; 1.28	1.31; 1.38; 1.26	1.29; 1.36; 1.46

diameter of the monolith Si-20-20 featuring 20 μm of macropore diameter by SEM and Hg porosimetry and 12.4 μm by micro-CT. At 50% of the macropore diameter distribution, the macropore diameters were distributed from 6 to 20 μm by micro-CT (**Figure 5**), and from 18 to 24 μm by Hg porosimetry (**Figure 4**). This difference could be explained by two assumptions: (1) micro-CT used a pore size distribution

expressed in numbers whereas Hg porosimetry used a distribution in pore volumes, which overestimated the contribution of the largest pores; (2) micro-CT tomography modeled pores with equivalent cylinders, which underestimates the maximum pore diameter.

The silica monoliths of 0.6 cm diameter with different macro- and mesopore diameters were cut at the desired length (0.5 cm) and grafted with amino functions to immobilize enzymes.

Functionalization of Silica Monoliths With Amino Groups

The surfaces of the silica monoliths with different meso- and macropore diameters and specific surface areas (**Table 2**) were functionalized by amino groups by silanization with aminopropyltriethoxy silane in ethanol at 80°C in batch. The excess of grafting agent in solution was set at 10 NH_2 per nm^2. The amount of grafted amino groups was calculated by TGA (**Supplementary Figure S5**) and confirmed by elemental analysis. The amount of grafted species expressed in mmol g^{-1} increased linearly with the increase of the specific surface area (**Figure 6**),

FIGURE 6 | Amount of aminopropyl groups grafted on silica monoliths as a function of their specific surface area.
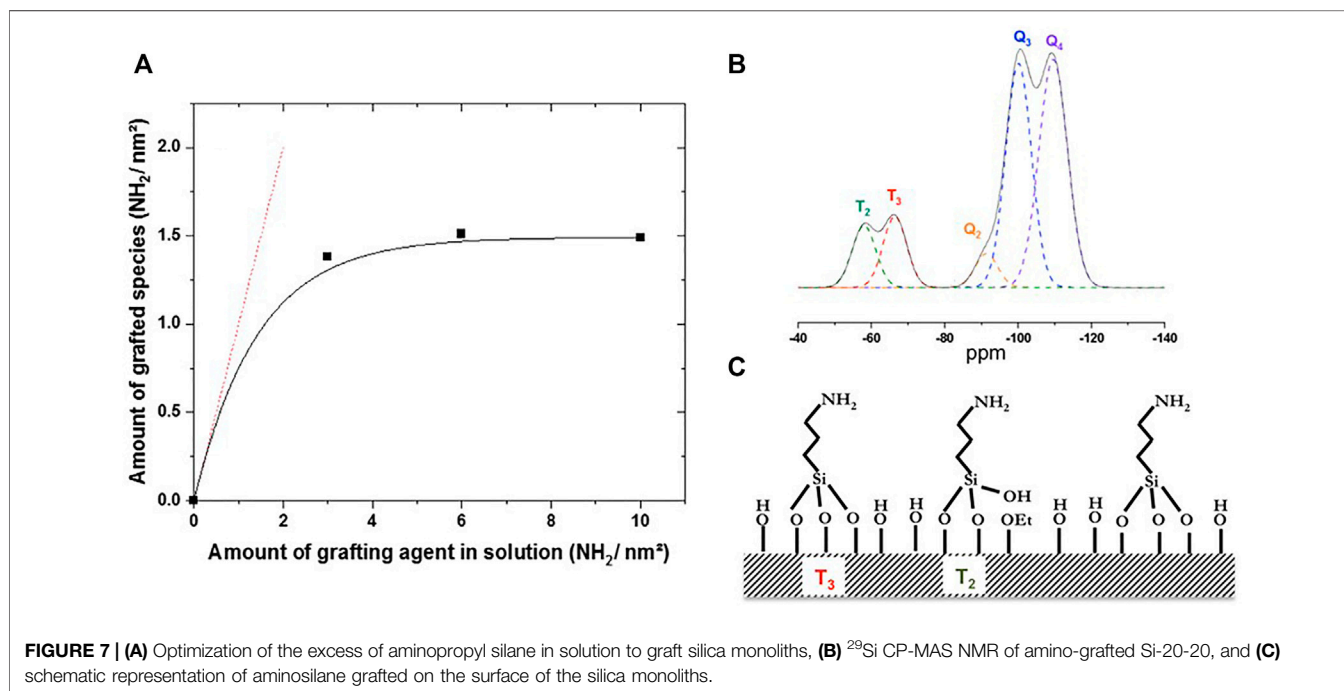
corresponding to a constant density of amino groups (1.1–1.5 NH_2 per nm^2) at the surface of the monoliths. ^{29}Si and ^{13}C MAS NMR confirmed the covalent grafting process with organosilanes grafted by 2 and 3 Si-O-Si bonds in an equivalent proportion [44% T_2 $(SiO)_2(HO)$-Si-R, 56% T_3 $(SiO)_3$-Si-R] (**Figure 7; Supplementary Figures S6, S7**). Some remaining ethoxy groups were noticed coming either from the pristine organosilane or from the EtOH washings (**Supplementary Figure S7**). After cladding the monoliths at 180°C the weight loss of organics slightly decreased (**Supplementary Figures S5**), probably due to the loss of these weakly attached ethoxy groups.
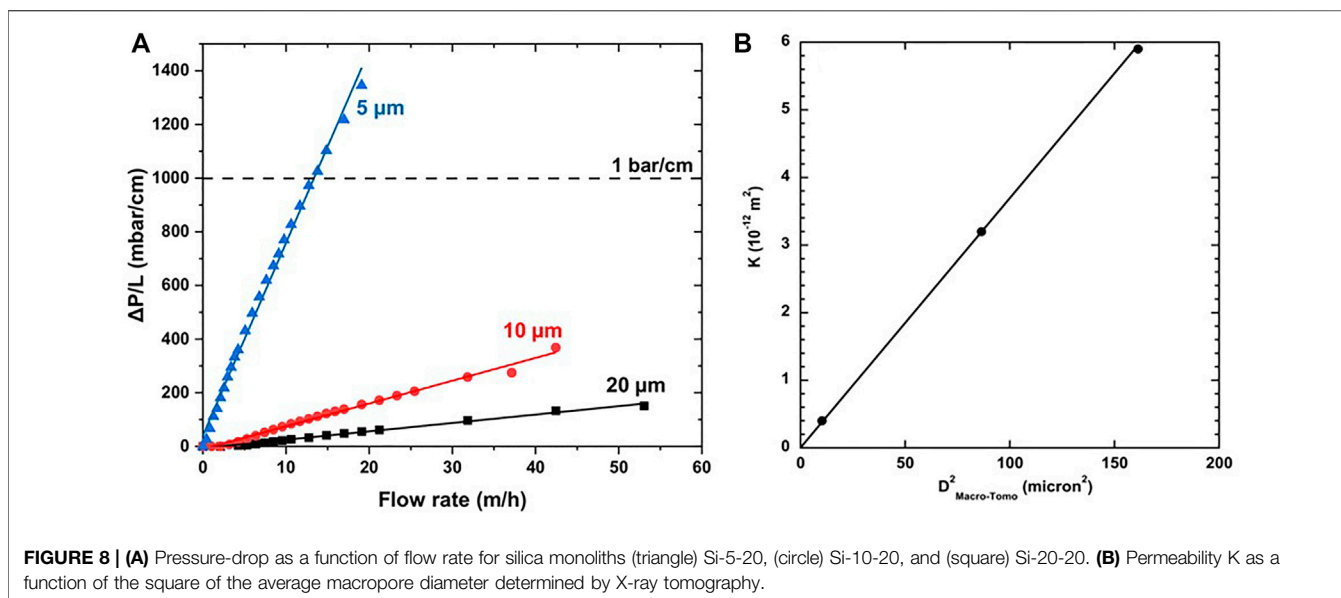
An optimization of the excess of grafting agent used in solution was followed for the monolith Si-20-20. A similar amount of grafted amino groups (1.5 NH_2 per nm^2, 0.83 mmol per g SiO_2-NH_2 monolith) was achieved for an excess of only 3 NH_2 per nm^2 (**Figure 7**). This optimization could reduce the cost of the process.

Permeability Tests

The amino-grafted silica monoliths (0.6 cm diameter, 0.5 cm length) with three different macropore diameters (5, 10, and 20 μm) and the same mesopore diameter (20 nm) (Si-5-20, Si-10-20, and Si-20-20) were cladded with a transparent FEP gain at 180°C. Water at 25°C was flowed through the monoliths with an increasing flow rate from 1 to 20 ml min^{-1}. The upstream pressure increased linearly for three monoliths: from 0.005 to 0.3 bar for the monoliths with 10 and 20 μm macropore diameter and reached 1 bar for the monolith featuring 5 μm macropore diameter. To examine the results, the flow rate in mL min^{-1} was expressed in linear flow rate in m h^{-1} by dividing the flow rate by the section of the monolith and the backpressure was expressed by unit of length divided by the measured pressure by the length of the monolith (**Figure 8**). The linear increase of the pressure drop as a function of the lineic flow rate evidenced that the flow is laminar as it follows the Darcy law (**Eq. 4**). Therefore, the permeability coefficients (K) of the silica monoliths were calculated from the slope of the linear relationship (**Eq. 4**) and were equal to 5.9×10^{-12}, 3.25×10^{-12}, and $0.39 \times 10^{-12}\,m^2$ for the monoliths featuring 20, 10, and 5 μm macropore diameters, respectively. The permeability coefficients were proportional to the square of the macropore diameter determined by micro-CT (**Figure 6**; **Table 3**):

$$K = \frac{D_{macro}^2}{27.4} \tag{5}$$

FIGURE 7 | (A) Optimization of the excess of aminopropyl silane in solution to graft silica monoliths, **(B)** ^{29}Si CP-MAS NMR of amino-grafted Si-20-20, and **(C)** schematic representation of aminosilane grafted on the surface of the silica monoliths.

FIGURE 8 | (A) Pressure-drop as a function of flow rate for silica monoliths (triangle) Si-5-20, (circle) Si-10-20, and (square) Si-20-20. **(B)** Permeability K as a function of the square of the average macropore diameter determined by X-ray tomography.

This result was very close to the one predicted by Hagen-Poiseuille law for a cylindrical tube:

$$K = \frac{D^2}{32} \quad (6)$$

Even if the macropores of the monoliths were tortuous, they almost acted as straight cylinders.

In porous media formed by packed particles, an empirical relationship was proposed as a function of the porosity of the media and the tortuosity of the pores (**Eq. 7**) assuming a cylindrical shape of pores (Lake et al., 1989):

$$K = \frac{D^2}{32} \frac{\varepsilon}{\tau} \quad (7)$$

However, for the monoliths, the resulting relationship gave a different result:

$$K = \frac{D^2 \varepsilon_{macro}}{14.3 \, \tau_Z} \text{ or } K = \frac{D^2 \varepsilon_{macro}}{13.5 \, \tau_m} \quad (8)$$

where τ_z is the tortuosity along the z-axis and τ_m is the mean tortuosity in the 3 directions.

It seemed that monoliths with similar macropore diameter as a packed-bed featured permeability twice higher.

A relationship including a derivation of **Eq. 7** adding an empirical geometric factor c for pore diameter (Panda et al., 1994) was proposed:

$$K = c \frac{D^2}{32} \frac{\varepsilon}{\tau} \quad (9)$$

In the case of the monoliths, this c parameter was 2.23 for the tortuosity along the z-axis or 2.37 for the average tortuosity in the three space directions.

Monoliths prepared by spinodal decomposition featured excellent permeability, close to cylindrical straight macropores,
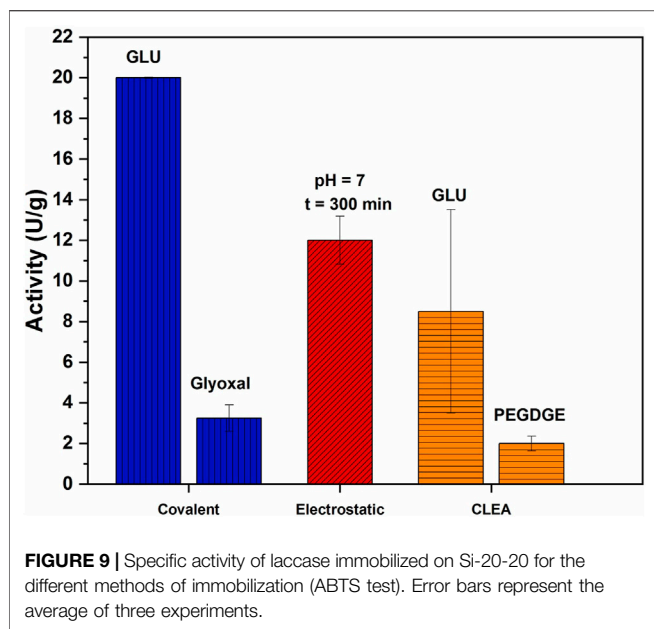
due to their outstanding network of homogeneous macropores totally interconnected. For catalytic and adsorption processes, a pressure drop of less than 1 bar cm^{-1} is required in industrial processes. The monoliths with the highest permeability were selected for the further biocatalytic processes under flow. It is worth noticing that no change of permeability was observed after enzyme immobilization. The permeability is mainly governed by the flow in the macropores and is not influenced by the diffusion inside the mesopores.

Immobilization of Laccases on Silica Monoliths
Methods of Enzyme Immobilization

Reactors formed by silica monoliths (0.6 cm diameter, 0.5 cm length, 50 mg) grafted with amino function (1.5 NH$_2$ per nm^2) and cladded with FEP gains at 180°C were used for laccase immobilization following 3 methods: (1) covalent grafting by coupling with GLU or glyoxal, (2) electrostatic interactions, and (3) adsorption followed by reticulation into the mesopores with cross-linkers as GLU or PEGDGE (CLEA method) (**Figure 1**). For the comparison of the different methods of enzyme immobilization, the monolith Si-20-20 was chosen.
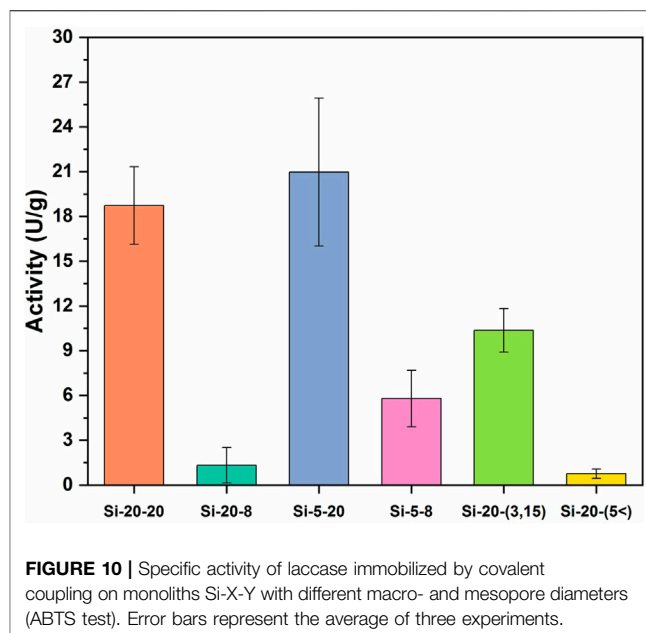
The laccase immobilization by adsorption and electrostatic interactions was the easiest method. The isoelectric point of laccase was PI = 4 (Kołodziejczak-Radzimska et al., 2020). The pKa of amino functions was approximately 10 (Gascon et al., 2014). The lipase immobilization was therefore performed at pH 5 and 7 to remain in the domain of pH stability of the enzyme and to get a negative charge on the enzyme and a positive charge on the amino groups (**Figure 1**, **Supplementary Figure S8**). Two durations of contact times were used: 90 and 300 min. The biocatalytic activity of the immobilized enzyme was measured on crushed monoliths with the ABTS test. The highest activity (12 U g^{-1}) was reached for an immobilization performed at pH 7 for 300 min (**Supplementary Figure S8**).

FIGURE 9 | Specific activity of laccase immobilized on Si-20-20 for the different methods of immobilization (ABTS test). Error bars represent the average of three experiments.

FIGURE 10 | Specific activity of laccase immobilized by covalent coupling on monoliths Si-X-Y with different macro- and mesopore diameters (ABTS test). Error bars represent the average of three experiments.

The covalent grafting with glutaraldehyde (GLU) as cross-linker was performed in two steps. First, a solution of GLU was flowed through the amino-silica monolith at pH 7 and allowed to react for 30 min. The white monolith turned into an orange color characteristic of the reaction of the addition of the aldehyde functions of GLU with the NH_2 functions (**Figure 1**). Secondly, the solution of enzyme was added at pH 7 and allowed to react for 60 min. The same procedure was performed with another less toxic cross-linker, i.e., glyoxal. The biocatalytic activities of the enzymes covalently bonded were 20 and 3 U g^{-1} for GLU and glyoxal, respectively (**Figure 9**). GLU had a beneficial effect on the enzyme activity, maybe by insuring a highest mobility of the enzyme due to the longer linker (five carbons for GLU instead of two for glyoxal).

The cross-linking of enzyme aggregates (CLEA method) into the mesopores was performed by adding first the enzyme solution at pH 7 for 90 min to immobilize the enzymes inside the mesopores and then GLU to reticulate the enzymes between them inside the mesopores (**Figure 1**). A similar procedure was used with another reticulating agent PEGDGE, which was introduced in the monolith at the same time as the enzyme solution, as the reactivity of PEGDGE is much slower than GLU (Baccour et al., 2020). The PEGDGE linker was chosen as it was shown to be very efficient to increase the stability and the activity of enzymes such as dehydrogenases (Baccour et al., 2020). The biocatalytic activities of the enzymes immobilized by CLEA methods were 9 and 2 U g^{-1} for GLU and PEGDGE, respectively (**Figure 9**). GLU had again a beneficial effect on the laccase activity. One may assume that the effect of the linker on activity is enzyme-dependent.

The highest laccase activity was obtained using the covalent bonding method with GLU as cross-linker with an activity of 20 U g^{-1}. The lowest activity of the enzymes in the CLEA proce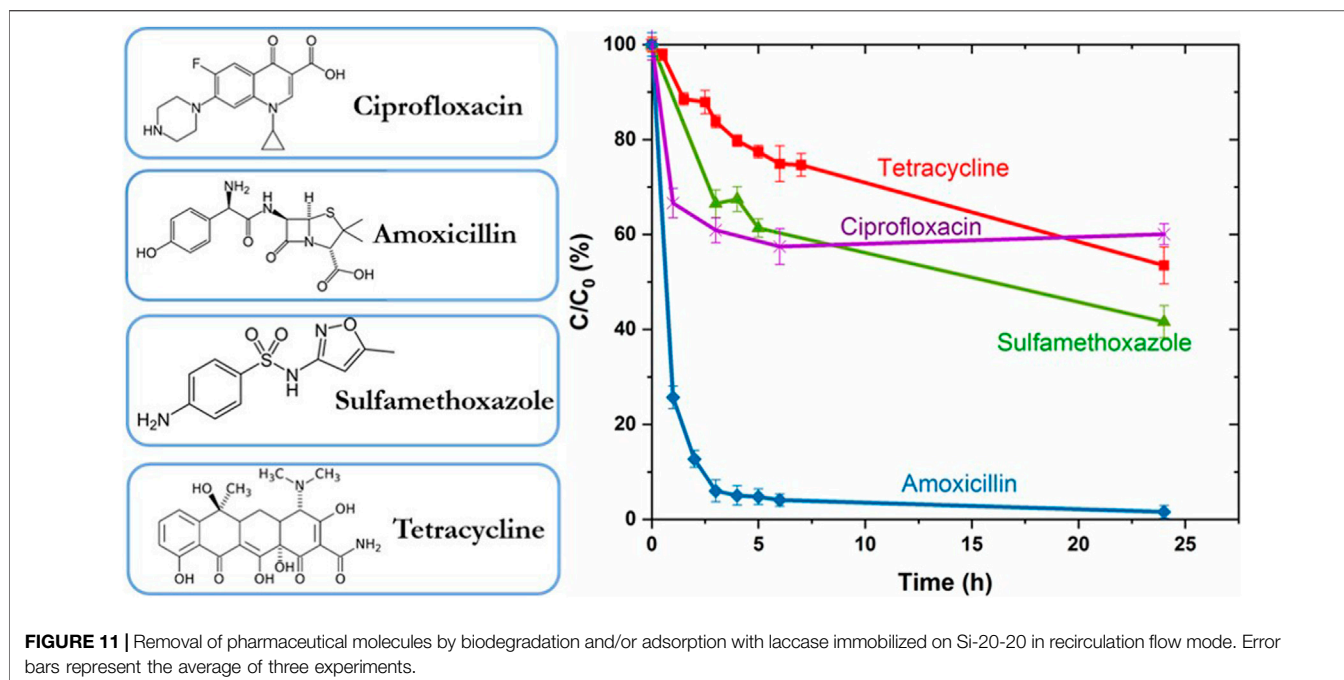dures may be the result of the rigidification of the laccases due to intramolecular cross-linking, which could reduce enzyme activity by decreasing the mobility of the catalytic site (Cabana et al., 2009). The covalent bonding method was retained for further laccase immobilization into the monoliths.

Influence of Silica Monoliths Pore Sizes on Enzyme Activity

Silica monoliths with different macropore and mesopore diameters (**Table 2**) and grafted with amino groups (**Figure 6**) were used as supports for laccase immobilization by covalent bonding with GLU as cross-linker (**Figure 1**). The macropore diameter of the monoliths had no influence on enzyme activity (**Figure 10**). However, the mesopore diameter was of prime importance. Laccase featured a kinetic diameter of approximately 6 nm (6.5 × 5.5 × 4.5 nm, MW 65 kDa), and the highest laccase activity (~20 U g^{-1}) was obtained for silica monoliths featuring the largest mesopore diameter of 20 nm (**Figure 10**). Without mesopores in the monolith, the enzyme activity was very low (~1 U g^{-1}) showing that the amount of enzymes grafted in the macropores is low in comparison to the amount of enzymes grafted in the mesopores. Thus, macropores played a minor role in the activity of the bioreactor.

The enzyme immobilization yield in silica monoliths featuring 20 nm mesopore diameter was calculated by **Eq. 2** and was 80 ± 5%. The immobilization efficiency calculated by **Eq. 3** was approximately 310%. Such an enhancement of the enzyme activity for immobilized enzymes was also reported for immobilized oxydoreductase (Boudrant et al., 2020). For monoliths featuring smaller mesopores, the immobilization yield was reduced. For example, for monoliths featuring mesopores of 8 nm diameter, the immobilization yield was approximately 55% ± 3%. Such a decrease in immobilization yield suggested a problem of accessibility of the enzymes by steric hindrance in very small mesopores. The immobilization

FIGURE 11 | Removal of pharmaceutical molecules by biodegradation and/or adsorption with laccase immobilized on Si-20-20 in recirculation flow mode. Error bars represent the average of three experiments.

efficiency was approximately 27%, suggesting also a problem of accessibility of the substrates to the catalytic sites of immobilized enzymes (Cabana et al., 2009). The enzyme should need space and mobility to express their activity. The monoliths Si-20-20 were retained as supports for enzyme immobilization for the flow biocatalytic process.

Stability on Storage of the Enzymes Immobilized in Silica Monoliths

The monoliths Si-20-20 functionalized with laccase were stored in the pH 7 buffer solution at 4°C. The activity of the immobilized enzymes was maintained for 15 days and was 80% after 30 days (**Supplementary Figure S9**). The free enzymes in buffer solution maintained more than 90% of their activity after 30 days. The small decrease of activity of the immobilized enzymes after 15 days of storage could be due to some hydrolysis of the Si-O-Si bonds and the liberation of a few enzymes.

Elimination of Pharmaceutical Micropollutants Found in Water in Continuous Flow

To analyze the efficiency of the immobilized laccase into monoliths for water treatment, different pharmaceutical molecules were chosen for their different properties of adsorption into materials and their different sensitivity towards oxidation processes. An aqueous solution (30 mL) containing 4 antibiotic molecules (ciprofloxacin, amoxicillin, sulfamethoxazole, and tetracycline) (**Figure 11**) at 20 ppm (mg L^{-1}) each was prepared in osmosed water at pH 6 and put in a reservoir. The reservoir was protected by an aluminum foil to prevent the molecules of light exposure and limit the risks of self-

degradation. Oxygen was bubbled into the reservoir in order to saturate the solution with oxygen. Pharmaceutical micropollutant depletion was carried out with three laccase-monolith reactors connected in series [0.6 cm diameter and 0.5 cm length with a biocatalytic (ABTS) activity of 5 U ± 0.5 U each]. The mixture of pharmaceutics was passed through the bioreactors at a flow rate of 1 mL min^{-1} (**Supplementary Figure S10**).

The depletion of the pharmaceutical molecules in continuous flow in a recycling mode was followed within time (**Figure 11**). Amoxicillin was rapidly eliminated at 95% in the first 3 h and totally eliminated after 24 h. Ciprofloxacin was eliminated at 40% in the first 3 h and no further elimination was noticed within time. Sulfamethoxazole was eliminated at 40% in the first 5 h and then the degradation rate decreased progressively and 60% of degradation was reached after 24 h. Tetracycline elimination was the slowest process with 25% elimination in the first 5 h reaching 55% after 24 h. To sum up, after 24 h of reaction process, the following remained in solution: 0 ppm of amoxicillin, 8 ppm of sulfamethoxazole, 9 ppm of tetracycline, and 14 ppm of ciprofloxacin.

The amount of pharmaceutics eliminated by adsorption or by self-degradation was determined with blank tests (**Supplementary Figure S11**). They were carried out after having deactivated the immobilized enzymes with a treatment of the reactor at 100°C for 10 min. The degradation of the pharmaceutical molecules was also followed in batch with free enzymes featuring the same initial biocatalytic activity of 0.5 U ml^{-1} (**Supplementary Figure S11**) to analyze the effect of the continuous flow process on the degradation rate of micropollutants.

Amoxicillin was demonstrated to be a sensitive molecule with an easy self-degradation by hydrolysis leading to 10%–20%

elimination after 24 h at pH 7 (Gozlan et al., 2013; Guardado et al., 2019). The blank test and the test with free enzymes gave a similar elimination of amoxicillin of 75% and 82%, respectively. It was therefore difficult to distinguish the contributions of enzymatic degradation, self-degradation, and adsorption on the removal of this molecule by laccase-monoliths. However, results with immobilized laccases have shown a higher level of elimination, close to 100%, demonstrating an efficient biocatalytic degradation of amoxicillin.

Unlike amoxicillin, ciprofloxacin is known to be a very stable molecule and recalcitrant towards biocatalytic processes (Guardado et al., 2019). Only 30% of ciprofloxacin was removed with the laccase-monolith (**Figure 11**). A similar result was obtained with the blank test with deactivated laccase (**Supplementary Figure S11**), and no elimination was observed with free laccase (**Supplementary Figure S11**). The removal of this molecule was thus due to its adsorption in silica monoliths.

In the case of tetracycline, 55% of elimination was noticed after 24 h with laccase immobilized on silica monoliths (**Figure 11**) and only 10% were adsorbed on deactivated monoliths (**Supplementary Figure S11**), demonstrating an efficient biocatalytic degradation of tetracycline by the immobilized laccases. The depletion level of tetracycline (55%) was similar to the one obtained for a solution containing only tetracycline without any other pharmaceutics (Ahmad et al., 2021). The presence of other micropollutants did not alter the action of the laccases towards tetracycline. However, the immobilized laccases were less efficient than free laccases, giving a degradation level for tetracycline as high as 95% (**Supplementary Figure S11**).

Sulfamethoxazole was previously presented as recalcitrant to the degradation by laccases with no elimination observed after 72 h of reaction at pH 7 (Guardado et al., 2019). However, in the present case, sulfamethoxazole was eliminated at 20% with free laccases (**Supplementary Figure S11**). This result was rather surprising because previous studies have shown that this molecule could only be partially degraded in the presence of redox mediators (Guardado et al., 2019; Guardado et al., 2021). Since no such compounds were added to our solution, it could be assumed that one or more degradation products of the other pharmaceutical molecules could act as redox mediators. As no such effects were observed for sulfamethoxazole degradation in the mixture of amoxicillin, sulfamethoxazole, ciprofloxacin, and carbamazepine (Guardado et al., 2021), the redox mediator could be a degradation product of tetracycline. The laccases immobilized in silica monoliths led to an even higher elimination of 60% of sulfamethoxazole. The blank test with deactivated laccases showed an elimination of 20% attributed to adsorption on silica monoliths. Therefore, laccases immobilized on silica monoliths showed a highly efficient biocatalytic activity. The covalent coupling of laccase on silica monolith enhanced the activity of the mediator coming from tetracycline degradation products.

The global depletion of pharmaceutics in water was 64% and 48% for immobilized and free laccases, respectively, showing the high potential of immobilized laccase on silica monoliths for water treatment under flow. The monoliths could be reused, as it was shown previously that its biocatalytic activity was maintained for at least five cycles for a solution containing only tetracycline (Ahmad et al., 2021).

CONCLUSION

Silica monoliths synthesized by spinodal decomposition and sol-gel process were prepared with different macropore and mesopore diameters for laccase immobilization. Different immobilization methods were compared, and the best method for laccase was the covalent binding of the enzymes on silica monoliths functionalized with amino groups through glutaraldehyde coupling. The highest activity of the laccase was found for the monoliths featuring the largest mesopore diameter (20 nm), surely due to the highest accessibility and mobility of the enzymes inside the mesopores, independently of the macropore diameter. The permeability of the monoliths was measured with water and the highest permeability was obtained for the monoliths featuring the largest macropore diameter (20 μm). Due to their high homogeneity of interconnected macropores, the flow in monoliths behaves almost as if the macropores were independent cylindrical straight pores. The silica monoliths of 20 μm macropore diameter and 20 nm mesopore diameter were revealed as the best support for laccase immobilization. These bioreactors were used to eliminate in continuous flow pharmaceuticals molecules classically found in different kind of waters. Due to the analytic techniques available in the laboratory, high amount of each pharmaceutics (20 mg L^{-1}) was used. The solution was passed through the bioreactors in a recirculation flow mode. After 24 h, amoxicillin was totally eliminated. Ciprofloxacin was eliminated at 30% due essentially to adsorption on the silica monolith. Tetracycline and sulfamethoxazole were eliminated at 55% and 60% due to mainly enzyme degradation with 10% and 20% of molecules possibly adsorbed on the monoliths, respectively. The immobilization of laccase on silica monoliths decreased the activity of laccases towards tetracycline degradation, but increased the biocatalytic activity of the laccases towards the degradation of amoxicillin and sulfamethoxazole. The global removal of pharmaceutics with immobilized laccases was 64%, whereas for free laccases, it was 48%, showing the high potential of these bioreactors. After 24 h, 20, 12, 9, and 8 mg L^{-1} of amoxicillin, sulfamethoxazole, tetracycline, and ciprofloxacin, respectively, were eliminated from the solution with immobilized laccases in flow. In real contaminated waters, considering that the amount of pharmaceutical molecules is much lower from ng L^{-1} to μg L^{-1}, this process could probably be used to totally eliminate efficiently these micropollutants at this level of concentrations.

DATA AVAILABILITY STATEMENT

The raw data supporting the conclusion of this article will be made available by the authors, without undue reservation.

AUTHOR CONTRIBUTIONS

WS and SA carried out the experiments, discussions and first draft writing. M-PB and NB contributed to the discussion, corrections, and writing. AB, PC, and CL contributed to x-ray tomography (experiments, discussion, and writing). AG and JS-M supervised the work, and contributed to discussion, writing, and corrections.

FUNDING

ACKNOWLEDGMENTS

SUPPLEMENTARY MATERIAL

The Supplementary Material for this article can be found online at: https://www.frontiersin.org/articles/10.3389/fceng.2022.823877/full#supplementary-material

REFERENCES

Ahmad, S., Sebai, W., Belleville, M.-P., Brun, N., Galarneau, A., and Sanchez-Marcano, J. (2021). Enzymatic Monolithic Reactors for Micropollutants Degradation. *Catal. Today* 362, 62–71. doi:10.1016/j.cattod.2020.04.048

Arca-Ramos, A., Kumar, V. V., Eibes, G., Moreira, M. T., and Cabana, H. (2016). Recyclable Cross-Linked Laccase Aggregates Coupled to Magnetic Silica Microbeads for Elimination of Pharmaceuticals from Municipal Wastewater. *Environ. Sci. Pollut. Res.* 23, 8929–8939. doi:10.1007/s11356-016-6139-x

Babin, J., Iapichella, J., Lefevre, B., Biolley, C., Bellat, J-P., Fajula, F., et al. (2007). MCM-41 Silica Monoliths with Independent Control of Meso – and Macroporosity. *New J. Chem.* 31, 1–11. doi:10.1039/b711544j

Baccour, M., Lamotte, A., Sakai, K., Dubreucq, E., Mehdi, A., Kano, K., et al. (2020). Production of Formate from CO2 Gas under Ambient Conditions: towards Flow-Through Enzyme Reactors. *Green. Chem.* 22, 3727–3733. doi:10.1039/d0gc00952k

Bebić, J., Banjanac, K., Ćorović, M., Milivojević, A., Simović, M., Marinković, A., et al. (2020). Immobilization of Laccase from Myceliophthora Thermophila on Functionalized Silica Nanoparticles: Optimization and Application in Lindane Degradation. *Chin. J. Chem. Eng.* 28, 1136–1144. doi:10.1016/j.cjche.2019.12.025

Björlenius, B., Ripszám, M., Haglund, P., Lindberg, R. H., Tysklind, M., and Fick, J. (2018). Pharmaceutical Residues Are Widespread in Baltic Sea Coastal and Offshore Waters - Screening for Pharmaceuticals and Modelling of Environmental Concentrations of Carbamazepine. *Sci. Total Environ.* 633, 1496–1509. doi:10.1016/j.scitotenv.2018.03.276

Boudrant, J., Woodley, J. M., and Fernandez-Lafuente, R. (2020). Parameters Necessary to Define an Immobilized Enzyme Preparation. *Process Biochem.* 90, 66–80. doi:10.1016/j.procbio.2019.11.026

Brady, D., and Jordaan, J. (2009). Advances in Enzyme Immobilisation. *Biotechnol. Lett.* 31, 1639–1650. doi:10.1007/s10529-009-0076-4

Bruce, G. M., Pleus, R. C., and Snyder, S. A. (2010). Toxicological Relevance of Pharmaceuticals in Drinking Water. *Environ. Sci. Technol.* 44, 5619–5626. doi:10.1021/es1004895

Burns, E. E., Carter, L. J., Kolpin, D. W., Thomas-Oates, J., and Boxall, A. B. A. (2018). Temporal and Spatial Variation in Pharmaceutical Concentrations in an Urban River System. *Water Res.* 137, 72–85. doi:10.1016/j.watres.2018.02.066

Cabana, H., Alexandre, C., Agathos, S. N., and Jones, J. P. (2009). Immobilization of Laccase from the white Rot Fungus Coriolopsis Polyzona and Use of the Immobilized Biocatalyst for the Continuous Elimination of Endocrine Disrupting Chemicals. *Bioresour. Technol.* 100, 3447–3458. doi:10.1016/j.biortech.2009.02.052

Carlsson, C., Johansson, A.-K., Alvan, G., Bergman, K., and Kühler, T. (2006). Are Pharmaceuticals Potent Environmental Pollutants? Part I: Environmental Risk Assessments of Selected Active Pharmaceutical Ingredients. *Sci. Total Environ.* 364, 67–87. doi:10.1016/j.scitotenv.2005.06.035

Davis, M. E. (2002). Ordered Porous Materials for Emerging Applications. *Nature* 417, 813–821. doi:10.1038/nature00785

de Cazes, M., Abejón, R., Belleville, M.-P., and Sanchez-Marcano, J. (2014a). Membrane Bioprocesses for Pharmaceutical Micropollutant Removal from Waters. *Membranes* 4, 692–729. doi:10.3390/membranes4040692

de Cazes, M., Belleville, M.-P., Petit, E., Llorca, M., Rodríguez-Mozaz, S., de Gunzburg, J., et al. (2014b). Design and Optimization of an Enzymatic Membrane Reactor for Tetracycline Degradation. *Catal. Today* 236, 146–152. doi:10.1016/j.cattod.2014.02.051

de Jongh, C. M., Kooij, P. J. F., de Voogt, P., and ter Laak, T. L. (2012). Screening and Human Health Risk Assessment of Pharmaceuticals and Their Transformation Products in Dutch Surface Waters and Drinking Water. *Sci. Total Environ.* 427-428, 70–77. doi:10.1016/j.scitotenv.2012.04.010

de Sousa Lima, L. F., and Mohallem, N. D. S. (2021). Nb2O 5/SiO2 Monoliths with Tailored Porosity: the Role of Polyethylene Glycol as Pore Modulating Agent. *J. Porous Mater.* 28, 361–367. doi:10.1007/s10934-020-00999-6

Debecker, D. P. (2018). Innovative Sol-Gel Routes for the Bottom-Up Preparation of Heterogeneous Catalysts. *Chem. Rec.* 18, 662–675. doi:10.1002/tcr.201700068

Demarche, P., Junghanns, C., Nair, R. R., and Agathos, S. N. (2012). Harnessing the Power of Enzymes for Environmental Stewardship. *Biotechnol. Adv.* 30, 933–953. doi:10.1016/j.biotechadv.2011.05.013

Didi, Y., Said, B., Micolle, M., Cacciaguerra, T., Cot, D., Geneste, A., et al. (2019). Nanocrystals FAU-X Monoliths as Highly Efficient Microreactors for Cesium Capture in Continuous Flow. *Microporous Mesoporous Mater.* 285, 185–194. doi:10.1016/j.micromeso.2019.05.012

Edwards, W., Leukes, W. D., and Bezuidenhout, J. J. (2002). Ultrafiltration of Petrochemical Industrial Wastewater Using Immobilised Manganese Peroxidase and Laccase: Application in the Defouling of Polysulphone Membranes. *Desalination* 149, 275–278. doi:10.1016/s0011-9164(02)00786-5

El Kadib, A., Chimenton, R., Sachse, A., Fajula, F., Galarneau, A., and Coq, B. (2009). Functionalized Inorganic Monolithic Microreactors for High Productivity in fine Chemicals Catalytic Synthesis. *Angew. Chem. Int. Ed. Engl.* 48, 4969–4972. doi:10.1002/anie.200805580

Fajula, F., Galarneau, A., and Renzo, F. D. (2005). Advanced Porous Materials: New Developments and Emerging Trends. *Microporous Mesoporous Mater.* 82, 227–239. doi:10.1016/j.micromeso.2005.01.036

Fernández-Fernández, M., Sanromán, M. Á., and Moldes, D. (2013). Recent Developments and Applications of Immobilized Laccase. *Biotechnol. Adv.* 31, 1808–1825. doi:10.1016/j.biotechadv.2012.02.013

Galarneau, A., Desplantier, D., Dutartre, R., and di Renzo, F. (1999). Micelle-templated Silicates as a Test Bed for Methods of Mesopore Size Evaluation. *Microporous Mesoporous Mater.* 27, 297–308. doi:10.1016/s1387-1811(98)00263-7

Galarneau, A., Mureseanu, M., Atger, S., Renard, G., and Fajula, F. (2006). Immobilization of Lipase on Silicas. Relevance of Textural and Interfacial Properties on Activity and Selectivity. *New J. Chem.* 30, 562–571. doi:10.1039/b517104k

Galarneau, A., Abid, Z., Said, B., Didi, Y., Szymanska, K., Jarzębski, A., et al. (2016a). Synthesis and Textural Characterization of Mesoporous and Meso-/macroporous Silica Monoliths Obtained by Spinodal Decomposition. *Inorganics* 4, 9. doi:10.3390/inorganics4020009

Galarneau, A., Sachse, A., Said, B., Pelisson, C.-H., Boscaro, P., Brun, N., et al. (2016b). Hierarchical Porous Silica Monoliths: A Novel Class of Microreactors for Process Intensification in Catalysis and Adsorption. *Comptes Rendus Chim.* 19, 231–247. doi:10.1016/J.CRCI.2015.05.017

Gascón, V., Márquez-Álvarez, C., and Blanco, R. M. (2014). Efficient Retention of Laccase by Non-covalent Immobilization on Amino-Functionalized Ordered Mesoporous Silica. *Appl. Catal. A: Gen.* 482, 116–126. doi:10.1016/j.apcata.2014.05.035

Gasser, C. A., Ammann, E. M., Shahgaldian, P., and Corvini, P. F.-X. (2014). Laccases to Take on the challenge of Emerging Organic Contaminants in Wastewater. *Appl. Microbiol. Biotechnol.* 98, 9931–9952. doi:10.1007/s00253-014-6177-6

Gozlan, I., Rotstein, A., and Avisar, D. (2013). Amoxicillin-degradation Products Formed under Controlled Environmental Conditions: Identification and Determination in the Aquatic Environment. *Chemosphere* 91, 985–992. doi:10.1016/j.chemosphere.2013.01.095

Grandclément, C., Seyssiecq, I., Piram, A., Wong-Wah-Chung, P., Vanot, G., Tiliacos, N., et al. (2017). From the Conventional Biological Wastewater Treatment to Hybrid Processes, the Evaluation of Organic Micropollutant Removal: a Review. *Water Res.* 111, 297–317. doi:10.1016/j.watres.2017.01.005

Guardado, A. L. P., Belleville, M.-P., Rostro Alanis, M. d. J., Parra Saldivar, R., and Sanchez-Marcano, J. (2019). Effect of Redox Mediators in Pharmaceuticals Degradation by Laccase: A Comparative Study. *Process Biochem.* 78, 123–131. doi:10.1016/j.procbio.2018.12.032

Guardado, A. L. P., Druon-Bocquet, S., Belleville, M.-P., and Sanchez-Marcano, J. (2021). A Novel Process for the Covalent Immobilization of Laccases on Silica Gel and its Application for the Elimination of Pharmaceutical Micropollutants. *Environ. Sci. Pollut. Res.* 28, 25579–25593. doi:10.1007/s11356-021-12394-y

Halling-Sørensen, B., Nielsen, S. N., Lanzky, P. F., Ingerslev, F., Lützhøft, H. C. H., and Jørgensen, S. E. (1998). Occurrence, Fate and Effects of Pharmaceutical Substances in the Environment-A Review. *Chemosphere* 36, 357–393.

Hartmann, M., and Kostrov, X. (2013). Immobilization of Enzymes on Porous Silicas - Benefits and Challenges. *Chem. Soc. Rev.* 42, 6277. doi:10.1039/c3cs60021a

Hou, C., Ghéczy, N., Messmer, D., Szymańska, K., Adamcik, J., Mezzenga, R., et al. (2019). Stable Immobilization of Enzymes in a Macro- and Mesoporous Silica Monolith. *ACS Omega* 4, 7795–7806. doi:10.1021/acsomega.9b00286

Iyer, P. V., and Ananthanarayan, L. (2008). Enzyme Stability and Stabilization-Aqueous and Non-Aqueous Environment. *Process Biochem.* 43, 1019–1032. doi:10.1016/j.procbio.2008.06.004

Jesionowski, T., Zdarta, J., and Krajewska, B. (2014). Enzyme Immobilization by Adsorption: a Review. *Adsorption* 20, 801–821. doi:10.1007/s10450-014-9623-y

Ji, C., Hou, J., Wang, K., Zhang, Y., and Chen, V. (2016). Biocatalytic Degradation of Carbamazepine with Immobilized Laccase-Mediator Membrane Hybrid Reactor. *J. Membr. Sci.* 502, 11–20. doi:10.1016/j.memsci.2015.12.043

Ji, C., Nguyen, L. N., Hou, J., Hai, F. I., and Chen, V. (2017). Direct Immobilization of Laccase on Titania Nanoparticles from Crude Enzyme Extracts of P. Ostreatus Culture for Micro-pollutant Degradation. *Sep. Purif. Technol.* 178, 215–223. doi:10.1016/j.seppur.2017.01.043

Jones, O. A., Lester, J. N., and Voulvoulis, N. (2005). Pharmaceuticals: a Threat to Drinking Water? *Trends. Biotechnol.* 23, 163–167. doi:10.1016/j.tibtech.2005.02.001

Kołodziejczak-Radzimska, A., Budna, A., Ciesielczyk, F., Moszynski, D., and Jesionowski, T. (2020). Laccase from Trametes Versicolor Supported onto Mesoporous Al₂O₃: Stability Tests and Evaluations of Catalytic Activity. *Process Biochem.* 95, 71–80.

Kowalczykiewicz, D., Przypis, M., Mestrom, L., Kumpf, A., Tischler, D., Hagedoorn, P.-L., et al. (2022). Engineering of Continuous Bienzymatic cascade Process Using Monolithic Microreactors - in Flow Synthesis of Trehalose. *Chem. Eng. J.* 427, 131439. doi:10.1016/j.cej.2021.131439

Kumar, V. V., and Cabana, H. (2016). Towards High Potential Magnetic Biocatalysts for On-Demand Elimination of Pharmaceuticals. *Bioresour. Technol.* 200, 81–89. doi:10.1016/j.biortech.2015.09.100

Lake, L. W. (1989). *Enhanced Oil Recovery: Englewood Cliffs*. New Jersey, NY: Prentice Hall, 550.

Linares, N., Hartmann, S., Galarneau, A., and Barbaro, P. (2012). Continuous Partial Hydrogenation Reactions by Pd@unconventional Bimodal Porous Titania Monolith Catalysts. *ACS Catal.* 2, 2194–2198. doi:10.1021/cs3005902

Lu, X., Hasegawa, G., Kanamori, K., and Nakanishi, K. (2020). Hierarchically Porous Monoliths Prepared via Sol-Gel Process Accompanied by Spinodal Decomposition. *J. Sol-gel Sci. Technol.* 95, 530–550. doi:10.1007/s10971-020-05370-4

Luckarift, H. R., Spain, J. C., Naik, R. R., and Stone, M. O. (2004). Enzyme Immobilization in a Biomimetic Silica Support. *Nat. Biotechnol.* 22, 211–213. doi:10.1038/nbt931

Mohammadi, M., As'habi, M. A., Salehi, P., Yousefi, M., Nazari, M., and Brask, J. (2018). Immobilization of Laccase on Epoxy-Functionalized Silica and its Application in Biodegradation of Phenolic Compounds. *Int. J. Biol. Macromol.* 109, 443–447. doi:10.1016/j.ijbiomac.2017.12.102

Naghdi, M., Taheran, M., Brar, S. K., Kermanshahi-Pour, A., Verma, M., and Surampalli, R. Y. (2017). Immobilized Laccase on Oxygen Functionalized Nanobiochars through mineral Acids Treatment for Removal of Carbamazepine. *Sci. Total Environ.* 584-585, 393–401. doi:10.1016/j.scitotenv.2017.01.021

Nakanishi, K., and Tanaka, N. (2007). Sol-Gel with Phase Separation. Hierarchically Porous Materials Optimized for High-Performance Liquid Chromatography Separations. *Acc. Chem. Res.* 40, 863–873. doi:10.1021/ar600034p

Panda, M. N., and Lake, L. W. (1994). Estimation of Single-Phase Permeability From Parameters of Particle-Size Distribution. *AAPG Bull.* 78, 1028–1039.

Patel, S. K. S., Kalia, V. C., Choi, J.-H., Haw, J.-R., Kim, I.-W., and Lee, J. K. (2014). Immobilization of Laccase on SiO₂ Nanocarriers Improves its Stability and Reusability. *J. Microbiol. Biotechnol.* 24, 639–647. doi:10.4014/jmb.1401.01025

Pype, R., Flahaut, S., and Debaste, F. (2019). On the Importance of Mechanisms Analysis in the Degradation of Micropollutants by Laccases: The Case of Remazol Brilliant Blue R. *Environ. Technol. Innovat.* 14, 100324.

Rajapaksha, A. U., Dilrukshi Premarathna, K. S., Gunarathne, V., Ahmed, A., and Vithanage, M. (2019). "Sorptive Removal of Pharmaceutical and Personal Care Products from Water and Wastewater," in *Pharmaceuticals and Personal Care Products: Waste Management and Treatment Technology.* Editors M. N. V. Prasad, M. Vithanage, and A. Kapley (Butterworth-Heinemann), 213–238. doi:10.1016/B978-0-12-816189-0.00009-3

Rocha, L. S., Pereira, D., Sousa, É., Otero, M., Esteves, V. I., and Calisto, V. (2020). Recent Advances on the Development and Application of Magnetic Activated Carbon and Char for the Removal of Pharmaceutical Compounds from Waters: A Review. *Sci. Total Environ.* 718, 137272. doi:10.1016/j.scitotenv.2020.137272

Rodrigues, R. C., Berenger-Murcia, A., Carballares, D., Morellon-Sterling, R., and Fernandez-Lafuente, R. (2021). Stabilization of Enzymes via Immobilization: Multipoint Covalent Attachment and Other Stabilization Strategies. *Biotechnol. Adv.* 52, 107821. doi:10.1016/j.biotechadv.2021.107821

Rouquerol, F., Luciani, L., Llewellyn, P., Denoyel, R., and Rouquerol, J. (2003). Texture des matériaux pulvérulents ou poreux. *Tech. Ing., TA* 3, 1050.1–1050.27.

Sadeghzadeh, S., Ghobadi Nejad, Z., Ghasemi, S., Khafaji, M., and Borghei, S. M. (2020). Removal of Bisphenol A in Aqueous Solution Using Magnetic Cross-Linked Laccase Aggregates from Trametes Hirsuta. *Bioresour. Technol.* 306, 123169. doi:10.1016/j.biortech.2020.123169

Sheldon, R. A., and van Pelt, S. (2013). Enzyme Immobilisation in Biocatalysis: Why, what and How. *Chem. Soc. Rev.* 42, 6223–6235. doi:10.1039/c3cs60075k

Sheldon, R. A. (2007). Enzyme Immobilization: the Quest for Optimum Performance. *Adv. Synth. Catal.* 349, 1289–1307. doi:10.1002/adsc.200700082

Shraddha, Shekher, R., Sehgal, S., Kamthania, M., and Kumar, A. (2011). Laccase: Microbial Sources, Production, Purification, and Potential Biotechnological Applications. *Enzyme Res.* 2011, 1–11. doi:10.4061/2011/217861

Silva, C., Silva, C. J., Zille, A., Guebitz, G. M., and Cavaco-Paulo, A. (2007). Laccase Immobilization on Enzymatically Functionalized Polyamide 6,6 Fibres. *Enzyme Microb. Technol.* 41, 867–875. doi:10.1016/j.enzmictec.2007.07.010

Singh Arora, D., and Kumar Sharma, R. (2010). Ligninolytic Fungal Laccases and Their Biotechnological Applications. *Appl. Biochem. Biotechnol.* 160, 1760–1788. doi:10.1007/s12010-009-8676-y

Strub, D. J., Szymańska, K., Hrydziuszko, Z., Bryjak, J., and Jarzębski, A. B. (2019). Continuous Flow Kinetic Resolution of a Non-equimolar Mixture of

Diastereoisomeric Alcohol Using a Structured Monolithic Enzymatic Microreactor. *React. Chem. Eng.* 4, 587–594. doi:10.1039/C8RE00177D

Szymańska, K., Pudło, W., Mrowiec-Białoń, J., Czardybon, A., Kocurek, J., and Jarzębski, A. B. (2013). Immobilization of Invertase on Silica Monoliths with Hierarchical Pore Structure to Obtain Continuous Flow Enzymatic Microreactors of High Performance. *Microporous Mesoporous Mater.* 170, 75–82. doi:10.1016/j.micromeso.2012.11.037

Szymańska, K., Odrozek, K., Zniszczoł, A., Torrelo, G., Resch, V., Hanefeld, U., et al. (2016a). MsAcT in Siliceous Monolithic Microreactors Enables Quantitative Ester Synthesis in Water. *Catal. Sci. Technol.* 6, 4882–4888. doi:10.1039/C5CY02067K

Szymańska, K., Pietrowska, M., Kocurek, J., Maresz, K., Koreniuk, A., Mrowiec-Białoń, J., et al. (2016b). Low Back-Pressure Hierarchically Structured Multichannel Microfluidic Bioreactors for Rapid Protein Digestion - Proof of Concept. *Chem. Eng. J.* 287, 148–154. doi:10.1016/j.cej.2015.10.120

Taghizadeh, T., Talebian-Kiakalaieh, A., Jahandar, H., Amin, M., Tarighi, S., and Faramarzi, M. A. (2020). Biodegradation of Bisphenol A by the Immobilized Laccase on Some Synthesized and Modified Forms of Zeolite Y. *J. Hazard. Mater.* 386, 121950. doi:10.1016/j.jhazmat.2019.121950

Tavares, A. P. M., Silva, C. G., Dražić, G., Silva, A. M. T., Loureiro, J. M., and Faria, J. L. (2015). Laccase Immobilization over Multi-Walled Carbon Nanotubes: Kinetic, Thermodynamic and Stability Studies. *J. Colloid Interf. Sci.* 454, 52–60. doi:10.1016/j.jcis.2015.04.054

van den Biggelaar, L., Soumillion, P., and Debecker, D. P. (2017). Enantioselective Transamination in Continuous Flow Mode with Transaminase Immobilized in a Macrocellular Silica Monolith. *Catalysts* 7, 54. doi:10.3390/catal7020054

van den Biggelaar, L., Soumillion, P., and Debecker, D. P. (2019). Biocatalytic Transamination in a Monolithic Flow Reactor: Improving Enzyme Grafting for Enhanced Performance. *RSC Adv.* 9, 18538–18546. doi:10.1039/c9ra02433f

van der Helm, M. P., Bracco, P., Busch, H., Szymańska, K., Jarzębski, A. B., and Hanefeld, U. (2019). Hydroxynitrile Lyases Covalently Immobilized in Continuous Flow Microreactors. *Catal. Sci. Technol.* 9, 1189–1200. doi:10.1039/C8CY02192A

Yiu, H. H. P., and Wright, P. A. (2005). Enzymes Supported on Ordered Mesoporous Solids: a Special Case of an Inorganic-Organic Hybrid. *J. Mater. Chem.* 15, 3690. doi:10.1039/b506090g

Zdarta, J., Feliczak-Guzik, A., Siwińska-Ciesielczyk, K., Nowak, I., and Jesionowski, T. (2020). Mesostructured Cellular Foam Silica Materials for Laccase Immobilization and Tetracycline Removal: A Comprehensive Study.

Microporous Mesoporous Mater. 291, 109688. doi:10.1016/j.micromeso.2019.109688

Zhang, Y., Ge, J., and Liu, Z. (2015). Enhanced Activity of Immobilized or Chemically Modified Enzymes. *ACS Catal.* 5, 4503–4513. doi:10.1021/acscatal.5b00996

Zheng, F., Cui, B.-K., Wu, X.-J., Meng, G., Liu, H.-X., and Si, J. (2016). Immobilization of Laccase onto Chitosan Beads to Enhance its Capability to Degrade Synthetic Dyes. *Int. Biodeterior. Biodegrad.* 110, 69–78. doi:10.1016/j.ibiod.2016.03.004

Zhou, Z., and Hartmann, M. (2012). Recent Progress in Biocatalysis with Enzymes Immobilized on Mesoporous Hosts. *Top. Catal.* 55, 1081–1100. doi:10.1007/s11244-012-9905-0

Zhu, Y., Kaskel, S., Shi, J., Wage, T., and van Pée, K.-H. (2007). Immobilization of *Trametes versicolor* Laccase on Magnetically Separable Mesoporous Silica Spheres. *Chem. Mater.* 19, 6408–6413. doi:10.1021/cm071265g

Zielińska, K., Szymańska, K., Mazurkiewicz, R., and Jarzębski, A. (2017). Batch and In-Flow Kinetic Resolution of Racemic 1-(n-Acylamino)alkylphosphonic and 1-(n-Acylamino)alkylphosphinic Acids and Their Esters Using Immobilized Penicillin G Acylase. *Tetrahedron: Asymmetry* 28, 146–152. doi:10.1016/j.tetasy.2016.11.007